Applied Energy 415 (2026) 127814

Contents lists available at ScienceDirect

Applied Energy

journal homepage: www.elsevier.com/locate/apen

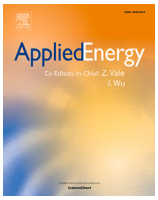

Bridging economics and physics in energy systems analysis: Effects of flexibility representation on model outcomes

Béla Wiegel [a,*], Jannis Eichenberg [b], Tizian Schug [c], Tim Hanke [d], Hannes Hobbie [b], Johannes Brunnemann [d], Christian Becker [a], Dominik Möst [b]

[a] Institute of Electrical Power and Energy Technology, Hamburg University of Technology, Harburger Schloßstraße 22A, Hamburg, 21079, Germany
[b] Chair of Business Administration, esp. Energy Economics, Dresden University of Technology, Dresden, 01069, Germany
[c] Institute for Operations Research and Information Systems, Hamburg University of Technology, Am Schwarzenberg-Campus 4, Hamburg, 21073, Germany
[d] XRG Simulation GmbH, Harburger Schlossstraße 6-12, Hamburg, 21079, Germany

HIGHLIGHTS

- Categorizing flexibility modeling depth and aggregation in optimization literature.
- Framework for analyzing optimization model accuracy with dynamic simulation.
- Online disaggregation algorithm for analyzing aggregated flexibility representation.
- Necessity of detailed prosumer models for accurate flexibility representation.
- Detailed physics outweigh aggregation in flexibility models.

ARTICLE INFO

Keywords:
Heat pump
Battery electric vehicle
Flexibility
Optimization models
Dynamic simulation

ABSTRACT

Efficiently decarbonizing fossil-based energy systems requires extensive electrification of end-users' heating and mobility sectors, alongside the provision of demand-side flexibility. Aggregators can harness this flexibility to enable cost-efficient supply in response to market incentives. While numerous studies address flexibility in energy systems, the underlying models conceptualize it in markedly different ways. This study, therefore, develops a meta-analytical modeling framework, derived from a systematic literature review, that couples market optimization with physics-based dynamic simulation to examine how varying the modeling depth and aggregation level of flexibility components, specifically heat pumps and battery electric vehicles, affects optimization results. Findings show that greater modeling depth yields more realistic optimization outcomes but at a higher computational cost. Endogenous heat pump coefficient-of-performance and storage modeling dampens price-arbitrage incentives and apparent flexibility, underscoring the need for detailed physical representation. Taking into account partial load behavior of electric cars avoids energy underprovisioning due to reduced efficiency. Aggregation level has only a minor influence when appropriate dispatch models are used. Transparent reporting of model depth, aggregation choices, and validation practices is thus crucial to ensure robust insights for utilities and policymakers.

1. Introduction

1.1. Motivation and background

Decarbonizing energy supply necessitates significant changes in electricity markets, both in terms of technological advancements as well as market design in fossil-dominated countries. The academic community has a broad consensus that achieving this transition requires a comprehensive increase in system flexibility to enable the further integration of weather-dependent renewable-based generation sources. Alongside the flexibilization of generation assets, demand-side technologies such as battery electric vehicles, battery storage, and power-to-heat solutions have attracted growing attention in recent years.

To provide policymakers with decision support on market design aspects and to develop operational and investment plans, academic entities and industry utilities widely employ electricity market and engineering models. Due to the growing rollout of flexible demand-side technologies,

* Corresponding author.
Email address: bela.wiegel@tuhh.de (B. Wiegel).

https://doi.org/10.1016/j.apenergy.2026.127814
Received 18 December 2025; Received in revised form 20 March 2026; Accepted 28 March 2026
Available online 23 April 2026

Nomenclature

Sets and indices

$i \in H$ Heat pumps or HP aggregates
$k \in K = \{1, \dots, k^{max}\}$ Discrete SOC sections
$t \in T = \{1, \dots, t^{last}\}$ Time steps
$v \in V$ Electric vehicles

Parameters

Δt Time step length (h)
η_v^{BEV} Linear efficiency factor (-)
η^{HP} Heat pump efficiency factor (-)
$\underline{soc}_{k,t}$ Lower bound of section k (K)
ε_t Flexibility range (kW)
ϑ_t^{amb} Ambient temperature (K)
$\vartheta^{BST,init}$ Initial BST temperature (K)
$\vartheta^{BST,\max}$ Maximum BST temperature (K)
$\vartheta_t^{BST,\min}$ Minimum BST temperature (K)
$avail_{v,t}$ Availability of BEV $\in \{0, 1\}$ (-)
c_p Specific heat capacity (J/(kg·K))
cap_v^{BEV} Maximum storage capacity (kWh)
$conv$ Conversion factor (K/kWh)
$cop_{k,t}$ COP of section k (-)
cop_t COP (exogenous) (-)
$dem_{v,t}^{BEV}$ Driving demand (kW)
dem_t^{HP} Heating demand (kW)
m^{BEV} Big-M constant ($\geq p^{BEV,nom}$) (-)
m^{HP} Big-M constant ($\geq \vartheta^{BST,\max}$) (-)
$mass$ Mass of the BST (kg)
$p_v^{BEV,nom}$ Nominal charging power (kW)
$p_v^{BEV,ob}$ On-board losses (kW)
$p_t^{HP,dem}$ Heat pump demand (kW)
$p^{HP,nom}$ Nominal power of HP (kW)
$sto_v^{BEV,init}$ Initial charging level (kWh)

Variables

$B_{v,t}$ Binary auxiliary variable (-)
COP_t^{QP} COP (endogenous) (-)
$P_{v,t}^{BEV}$ Charging power (kW)
$P_{k,t}^{HP}$ Power for section k (kW)
P_t^{HP} Heat pump power (kW)
Q_t Thermal output (kW)
SOC_t BST temperature at end of t (K)
$STO_{v,t}^{BEV}$ Storage level (kWh)
$Z_{k,t}$ Binary auxiliary variable (-)

these models must increasingly capture different forms of flexibility realistically to ensure profound assessments of market outcome and system reliability.

Despite its crucial importance, the representation of flexibility in these models varies considerably across applications and academic disciplines. Some models employ detailed technology-level formulations, such as single component representations with operation-state-dependent characteristics, to capture short-term operational dynamics, closely resembling underlying physics (e.g., [11], and [41]). Others rely on aggregated constraints or simplified representations, like virtual technology fleets with constant efficiencies (e.g., [4], and [7]), often due to computational challenges associated with complex decision-making faced by market stakeholders and/or non-linear relationships present between technological variables.

While a large body of research explores the various aspects of flexibility in energy systems, the models applied conceptualize flexibility in markedly different ways (see Section 2). There is only limited systematic understanding of how such conceptual differences influence model outcomes to date. A meta-analytical perspective can therefore support the comparison and interpretation of results across studies with varying flexibility representations, and is particularly valuable when these models inform utility strategies and policy decisions, which are highly relevant for future decarbonization efforts.

To address this gap, this study proposes an analytical framework that enables a structured comparison of flexibility representations and their implications for model-based insights into the operational behavior of battery electric vehicles and heat pumps within decentralized energy systems. Particular attention is devoted to these technologies, because their representation in models is especially challenging due to their distinct temporal dynamics and dispatch characteristics. The framework (Fig. 1) systematically links distinct flexibility concepts to their corresponding modeling approaches and analytically evaluates their impacts by coupling market-based and engineering-oriented models through quantitative metrics.

1.2. Analytical framework

The analytical framework comprises three layers: (a) *Classification of flexibility representation*, (b) *Model-based investigation*, and (c) *Evaluation of indicators*. In the first layer, flexibility representations identified through a structured literature analysis are classified according to their aggregation level (e.g., single component vs. virtual technology fleet) and component-level modeling depth (e.g., constant efficiency vs. operation-state-dependent characteristics). The second layer couples *engineering-oriented dynamic simulations* with *market-based optimization models* to systematically explore how different representations of flexibility affect dispatch decisions and resulting physical system behavior. In the third layer, *quantitative indicators* of the modeling domains, i.e., economic and technical indicators as well as indicators regarding model complexity are used to assess and compare the outcomes of the coupled model analyses. Together, these layers provide a coherent analytical structure for examining how modeling choices influence insights into the operational flexibility of distributed energy technologies.

1.3. Contribution

Building on this analytical framework, this study aims to support both academic and industry modelers in balancing model simplification against information gain, thereby enhancing the tractability and interpretability of power system analyses that inform ongoing decarbonization efforts. Specifically, the contributions of this study are threefold:

(a) developing a systematic classification scheme that categorizes flexibility representations according to technological component detail and technology-fleet aggregation level;
(b) proposing a disaggregation controller for Electric Heat Pumps (HPs) to enhance the accuracy of aggregated demand-side modeling; and
(c) evaluating alternative flexibility representations in a detailed case study on dispatch optimization, using performance indicators consistent with engineering, economics, and operations research practices.

The contributions of this study provide several key advances for energy system modeling and decision support. First, the proposed classification scheme establishes a common conceptual foundation that enables consistent comparison of flexibility representations across studies, thereby improving the interpretability and transferability of model-based insights. Second, the disaggregation controller enhances the

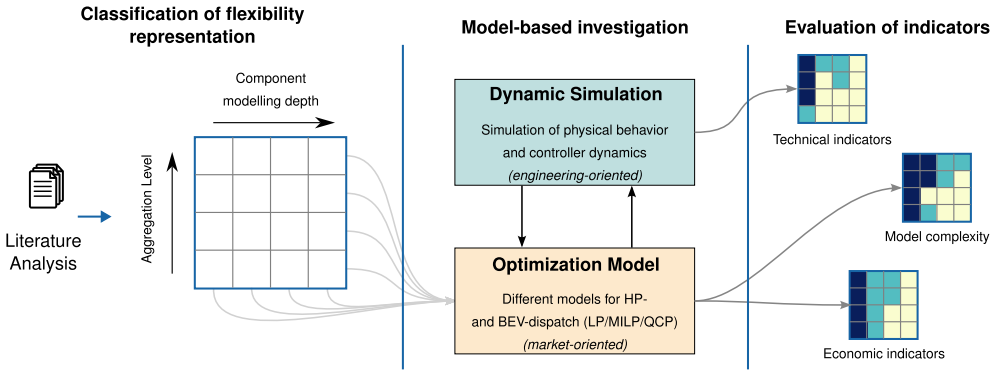

Fig. 1. Study approach.

practical applicability of aggregated demand-side models by reconciling computational tractability with operational accuracy, which is particularly relevant for large-scale energy system analyses. Third, the systematic evaluation of flexibility representations quantifies the trade-offs between model fidelity and complexity, offering actionable guidance for modelers from academia and industry stakeholders on selecting appropriate modeling approaches depending on the decision context.

The remainder of the paper is structured as follows. Section 2 reviews the relevant literature and develops the systematic classification scheme for types of flexibility representation in market-oriented optimization models. Section 3 presents the mathematical formulations of the different modeling alternatives and links market-oriented and engineering-based modeling tools. Section 4 introduces the case study that serves as a demonstration example, and Section 5 discusses the outcomes of the various representations based on techno-economic performance indicators. Finally, Section 6 concludes with recommendations for the academic modeling community and industry stakeholders.

2. Literature-based classification of optimization techniques in sector-coupling representations

The literature on energy system models varies significantly in physical detail. This chapter analyzes existing studies to identify the main approaches to component modeling depth and aggregation level. First, a classification scheme is developed to define different levels of physical detail in optimization models (Section 2.1). Next, the scheme is used to systematically categorize the published optimization models, thereby providing a clear overview of the level of physical detail employed in existing energy-system studies (Section 2.2).

2.1. Developing a flexibility classification scheme for optimization models

Large three-phase flexibility potentials in households are mainly provided by Battery Electric Vehicles (BEVs), Electric Heat Pumps (HPs), and battery storage systems. Since battery storage systems do not involve issues related to physical dynamics (e.g., dynamic coupling or catch-up effects), this study concentrates on the remaining flexibility sources.

As noted above, the level of physical detail for these flexibility options spans two dimensions, namely

1. component-modeling depth, and
2. aggregation level.

Table 1(a) presents the classification of BEV and HP models with respect to the first dimension. Thus, increasing n corresponds to a higher degree of fidelity for technical components (e.g., the accuracy of the COP-dependency approximation in HP models). Table 1(b) presents the second dimension, where increasing m corresponds to a higher aggregation level for groups of components (e.g., a fleet-level aggregation strategy for vehicles). In this paper, the notation $\mathrm{BEV}_{(n,m)}$ and $\mathrm{HP}_{(n,m)}$ is used to denote the classes defined in Table 1 and is employed consistently in all subsequent sections.

Table 1
Modeling depth classification for battery electric vehicles (BEVs) and heat pumps (HPs), separated into component model depth (n) and aggregation level (m). $T_{amb,t}$ refers to ambient temperatures.

Model	n/m	Classification description	Ref.
(a) Component model depth classification (n).			
$\mathrm{BEV}_{(n,\cdot)}$	1	Constant efficiency	[25]
	2	Constant eff. + Min. Power	–
	3	Efficiency curve + Min. Power	[51]
$\mathrm{HP}_{(n,\cdot)}$	1	Stylized HP (no COP)	[9]
	2	$COP \approx f(\varnothing_t T_{amb,t})$	[42]
	3	$COP \approx f(T_{amb,t})$	[52]
	4	$COP \approx f(SOC_t, T_{amb,t})$	[25]
	5	$COP = f(SOC_t, T_{amb,t})$	[11]
(b) Aggregation level classification (m).			
$\mathrm{BEV}_{(\cdot,m)}$	1	Single component model	[25]
	2	Swarm battery	[35]
	3	Virtual Storage	[38]
$\mathrm{HP}_{(\cdot,m)}$	1	Single component model	[25]
	2	Linear aggregation	[27]
	3	Insul. & storage cap.	[18]

With regard to Table 1(a), the physical representation of HP dynamics can vary greatly and range from a simplified model in which a specific electrical energy level must be reached by a particular time, disregarding the conversion to thermal energy ($\mathrm{HP}_{(1,\cdot)}$), to an exact representation of non-linear Coefficient of Performance (COP) and controller dynamics ($\mathrm{HP}_{(5,\cdot)}$). While linear COP approximations are limited to ambient temperature dependencies (see $T_{amb,t}$ in $\mathrm{HP}_{(2,\cdot)}$ and $\mathrm{HP}_{(3,\cdot)}$), non-linear extensions can model State of Charge (SOC)-dependent COP characteristics. These non-linearities can be linearized discretely ($\mathrm{HP}_{(4,\cdot)}$) or modeled exactly using quadratic constraints ($\mathrm{HP}_{(5,\cdot)}$). Both identified linear COP approximations differ in the resolution level of ambient temperature dependency: $\mathrm{HP}_{(2,\cdot)}$ is based on average temperature dependencies (e.g., over the course of a year), whereas $\mathrm{HP}_{(3,\cdot)}$ requires sharp temperature dependencies over time.

With regard to the aggregation level, a distinction is made between three different variants in the literature, as shown in Table 1(b). In addition to single-component models ($\mathrm{HP}_{(\cdot,1)}$), HP aggregation progresses through two stages: linear aggregation, where the energy demand depends solely on HP quantity (or top-down approaches) ($\mathrm{HP}_{(\cdot,2)}$), and advanced aggregation based on bottom-up household requirements ($\mathrm{HP}_{(\cdot,3)}$). In the latter, the aggregated COP depends on single-component storage capacities and insulation-dependent flow temperature, ensuring the required comfort at the household level even with higher aggregation level.

Base BEV models assume idealized behavior, where energy demand depends only on driving patterns, battery capacity, and maximum charging power ($BEV_{(1,\cdot)}$). Models incorporating a minimum charging power ($BEV_{(2,\cdot)}$) reflect additional real-world limitations. The final tier ($BEV_{(3,\cdot)}$) explicitly models non-linear efficiency curves depending on charging power. This includes energy losses during charging (e.g., online inefficiencies of on-board electronics and operating point dependent efficiencies of charging equipment), demonstrating that lower charging speeds amplify these losses [51]. Here, the model accounts for potentially decisive extra energy needed to offset slower charging, such as when a grid operator restricts consumption due to high line loadings in the distribution grid.

Beyond single-component models ($BEV_{(\cdot,1)}$), BEV aggregation can be approached naively via swarm battery implementation ($BEV_{(\cdot,2)}$) or accurately via virtual storage implementation ($BEV_{(\cdot,3)}$). The former is known to overestimate flexibility potential due to constraint relaxation in aggregation. As a result, naive aggregation allows to charge the swarm battery, from which even cars disconnected from the grid can draw their energy. The latter, however, preserves the solution space, thereby mitigating overestimation [38].

2.2. Categorizing literature-based optimization models using the flexibility classification scheme

41 exemplary papers,[1] ranging from single households optimizing their flexible loads against price signals to complex energy system models, were investigated to discuss the classification scheme regarding the frequency of modeling approaches used in the literature explained before. Thus, the classification scheme indicates if literature tends toward complex or simplified flexibility representations, varying with application and required level of detail. While 18 papers developed optimization models comprising BEVs, 28 modeled HPs. Figs. 2 and 3 organize the literature according to the newly introduced two-dimensional classification scheme.

Regarding Fig. 2, literature tends towards a low component modeling depth with regard to the representation of electromobility ($BEV_{(1,\cdot)}$). Except for one, all models using aggregation techniques implement a naive swarm battery and relate to $BEV_{(1,2)}$. One exception in [38] is solving the aggregation problem regarding overestimated flexibility, introducing a higher aggregation level based on an accurate virtual storage. In this study, the authors omit a comprehensive model-based analysis of BEV aggregation levels and refer to the findings of [38], indicating that a realistic flexibility potential ($BEV_{(1,3)}$) is 10 times lower than the naive aggregation ($BEV_{(1,2)}$). The focus in this study, instead, is to explore more detailed BEV models at the component level omitting aggregation-related investigations, and addressing the identified research gap.

While most HP models are located in the lower left corner of Fig. 3, only one model combines a high physical approximation quality with a high aggregation level ($HP_{(4,3)}$). In contrast to BEVs, HP models range from $HP_{(1,\cdot)}$ to $HP_{(4,\cdot)}$ and demonstrate a significant variance of component modeling depth. While exact formulations are poorly represented, all other approaches are proving more widespread. Notably, most models relate to $HP_{(2,\cdot)}$. They simplify linear COP dependencies, assuming constant ambient temperatures over time—often throughout the entire year. These models can be upgraded to the next higher category ($HP_{(3,\cdot)}$) by changing the input data without the need for model reformulation.

The literature analysis thus reveals a wide range of component modeling depths and aggregation levels. The following section presents a methodology that allows the implications of the various variants to be analyzed in detail and their significance to be classified.

[1] The search included terms like "*aggregator*", "*flexibility*", "*heat pump*", "*battery electric vehicle*", "*optimization*", and "*costs*".

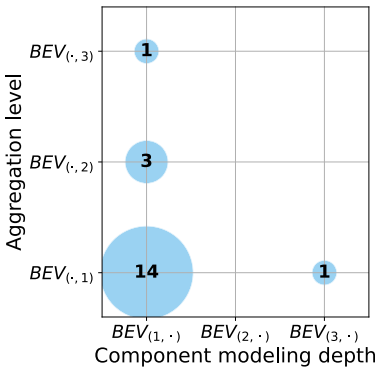

Fig. 2. Literature classification (BEV). $BEV_{(1,1)}$ [4,6,7,21,22,25,26,29,45,47–49,52,54]. $BEV_{(1,2)}$ [17,28,35]. $BEV_{(1,3)}$ [38]. $BEV_{(3,1)}$ [51] (This work adapts engineering based models.).

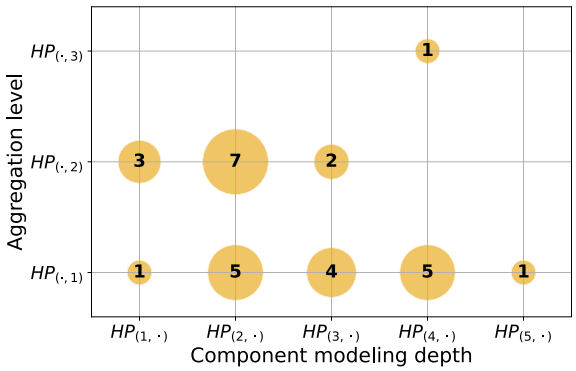

Fig. 3. Literature classification (HP). $HP_{(1,1)}$ [40]. $HP_{(2,1)}$ [8,10,12,15,42]. $HP_{(3,1)}$ [31,49,52,54]. $HP_{(4,1)}$ [25,30,32,41,55]. $HP_{(5,1)}$ [11]. $HP_{(1,2)}$ [5,9,37]. $HP_{(2,2)}$ [16,28,35,36,44,50,53]. $HP_{(3,2)}$ [17,23]. $HP_{(4,3)}$ [18].

3. Modeling framework

With the growing penetration of electrified consumers, i.e., HPs and BEVs, the flexibility potential in lower grid levels is increasing significantly. On the one hand, these flexibilities arise from process-related necessity, for example in the form of Buffer Storage Tanks (BSTs) in Building Heating Systems (BHSs) with HPs as heat source, and on the other hand, through a deliberate increase in flexibility to gain the ability to react to external influences and thus optimize operation.

If these inherent as well as created flexibilities are now exploited in the market to cover demand in a price-oriented and thus cost-reducing manner, physical effects arise within the components that do not occur during regular operation. These are typically operating point shift-related efficiency changes and subsequent catch-up effects. An example of this is the COP of HPs: if a low price phase leads to an operating point increase, system temperatures will rise together with a non-linear decrease of the COP, leading into a phase with decreased operating point of the HP due to BST dynamics.

The following analyses aim to evaluate various mathematical formulation approaches that take this behavior into account, thereby leading to a strategy that maps the flexibilities as precisely as possible with a sufficiently accurate modeling depth. Within the framework developed, a detailed engineering-oriented non-linear dynamic simulation of the energy system is combined with a market-oriented model to evaluate the implications of varying modeling depth.

The next subsections are structured as follows: Section 3.1 introduces the overarching model-coupling framework. Section 3.2 then details the engineering-oriented simulation domain, including the dynamic modeling of flexible technologies. Section 3.3 describes the interface used to transfer information from the engineering-oriented simulation to the

market-oriented optimization model. Finally, Section 3.4 presents the formulations applied to represent different component modeling depths within the optimization.

3.1. Modeling scheme: linking optimization and dynamic simulation

A key challenge in coupling optimization models with engineering-oriented dynamic simulations is to accurately represent catch-up effects arising inside the modeled technologies, as well as temporal effects arising from non-linear component behavior and control structures. To address this, a framework is being developed that integrates both modeling approaches (see Fig. 4). The framework consists of six main steps, explained below:

1. **Scenario**: The first step of the model coupling involves creating the scenario, configuring input data, and compiling the engineering-oriented simulation model. It establishes the foundation for all subsequent analyses by defining key parameters, boundary conditions, and structural assumptions.
2. **Simulation**: A dynamic simulation is performed in Modelica [3] using the TransiEnt-Library [20] with internal controllers active (*Mode A*). Each component controls itself autonomously, resulting in a demand profile typical of systems without centralized optimization, reflecting current practices in many real-world applications. This is referred to as customer baseline load.
3. **Aggregation**: The individual demand profiles and relevant system data are gained from the simulated customer baseline load. If aggregation is to be analyzed according to the selected model, individual time series are aggregated in this step. This enables the analysis of the effects introduced by the aggregation itself.
4. **Optimization**: The optimization model is implemented in GAMS based on the scenario's boundary conditions. In this step, the model to be examined is selected from the pool of identified models (compare Table 1), which is of particular importance for the next steps.
5. **Re-simulation and Disaggregation**: The optimized demand profile is then applied in a second simulation run of the dynamic models in Modelica. Here, the electricity demand is imposed directly on the components (*Mode B*), effectively bypassing their internal control systems to assess the impact of centralized optimization. If the effect of aggregation is analyzed and was applied in step 3, the disaggregation of the central signal into individual components must take place in this step.
6. **Validation**: To evaluate the adequacy of the optimization model in capturing the dynamic behavior of the system, a validation step is conducted. This involves comparing the results of the dynamic simulation with those obtained from the optimization. The analysis focuses on the temporal trajectories of selected state variables such as the SOC or system temperatures, which reflect the physical response of the system to control actions. By quantifying the deviations between simulated and optimized trajectories, a benchmark is established based on performance indicators that assess the representational fidelity and practical applicability of the optimization approach.

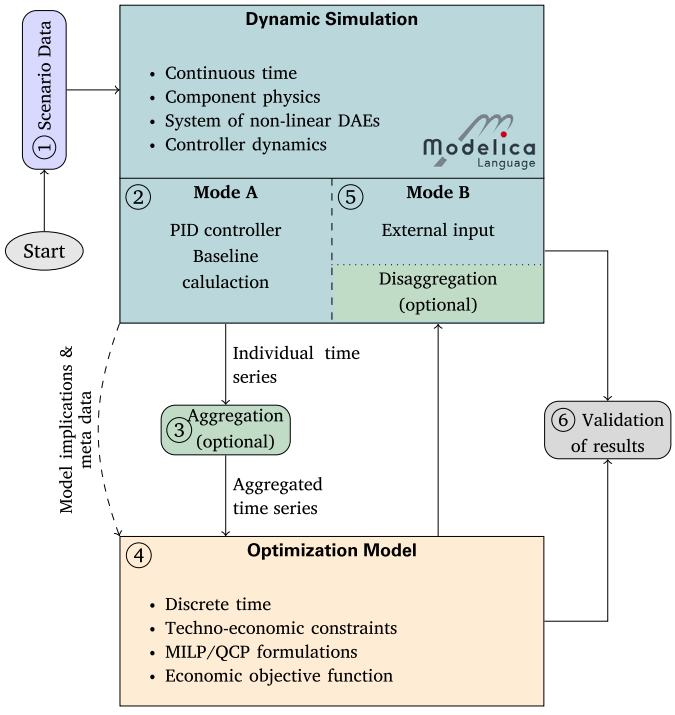

Fig. 4. Modeling scheme for coupling optimization with dynamic simulation.

To analyze the implications of varying component modeling depth, the following section first outlines the construction of the engineering-oriented simulation model. This is followed by a systematic presentation of the different flexibility formulations applied within the market-oriented optimization framework.

3.2. Engineering-oriented dynamic simulation model of flexible components

The following sections first describe the components considered in this paper, BEV and BHS, and their specifics for engineering-oriented modeling.

3.2.1. Battery electric vehicles

In residential settings, BEVs are typically charged upon arrival at the home charging station. Without any external control signals, the charging process starts immediately when the BEV is connected to the public grid and stops once the target SOC is reached. This behavior is represented accordingly in the dynamic simulation.

When modeling the energy demand, the charging efficiency plays a crucial role and must therefore be taken into account in the charging controller implemented within the dynamic model. Typically, the efficiency of the charging process for a BEV depends on the charging power [46]. In partial load operation, the efficiency is usually lower than at nominal load. This is due not only to power electronics that are typically optimized for a single operating point, which is the nominal charging power. Additionally, on-board electronics represent a constant auxiliary load during an active charging session. This continuous consumption becomes more significant during partial load operation, as the longer charging duration increases its relative impact.

As part of the ERIGrid 2.0 project [1], the authors conducted a measurement campaign at the SYSLAB test facility of the Technical University of Denmark (DTU). Several current BEV models were tested with respect to their charging efficiency [51]. The measurement results of the operating points are shown in Fig. 5, illustrating the reduced efficiency under partial load conditions. The measured efficiency curves are implemented in the charging controller that is part of the dynamic simulation. The figure also includes the result of an empirical model that approximates the efficiency. In this model $P^{bev}_{v,ob}$ represents the constant auxiliary load and η^{bev}_{v} the modeled converter efficiency[2]:

$$P^{bev}_{v,\mathrm{DC}} = \eta^{bev}_{v}\, P^{bev}_{v,\mathrm{AC}} - P^{bev}_{v,ob} \qquad \forall v \in V, \tag{1}$$

with V denoting the set of vehicles under consideration, $P^{bev}_{v,\mathrm{DC}}$ the power to the battery, and $P^{bev}_{v,\mathrm{AC}}$ the power taken from the grid.

[2] Reformulating the equation as $P^{bev}_{v,\mathrm{DC}}/P^{bev}_{v,\mathrm{AC}}$ yields a hyperbolic function, which is evaluated in Fig. 5.

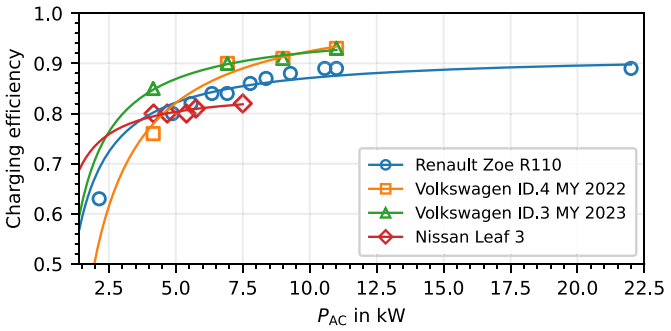

Fig. 5. Measured efficiency curves of different current BEV models.

As part of coupling the model domains, driving profiles with discrete events such as departures and returns, and thus the BEV's availability, are of particular importance. These events must be transferred from the time-continuous simulation to the discrete temporal resolution of the aggregator model. Two approaches can be distinguished:

- *Rounding*: Events in the first half of time slice are shifted to its beginning, and events in the second half are shifted to its end. This preserves the average event duration across many profiles but may overestimate flexibility, as the BEV can appear available when it is not.
- *Guaranteed presence*: The BEV is considered available only in time slices of full presence. This approach underestimates flexibility but ensures that procured energy can be consumed.

In this paper, the *Guaranteed presence* mode is applied since this makes sure that whenever the aggregator purchases energy, it can also be consumed by the BEV. This avoids implausibilities in the coupling framework.

After optimization, the resulting discretized charging strategy must be transferred back into the time-continuous domain. Two approaches are available for this purpose, illustrated in Fig. 6:

- *Direct mapping*: The hourly energy purchase is directly converted into a constant power and passed to the dynamic simulation. In this mode, no changes are made to the time series.
- *Condensed time series with rated power*: Here, it is necessary to distinguish the duration of a charging session. Suppose the BEV charges as a single event within one hour at partial load. In that case, it is charged with rated power at the beginning of the event in the simulation until the amount of energy procured by the aggregator for this charging event is reached. If the charging event spans multiple hours, the outer hours are adjusted relative to the event boundaries, such that charging occurs during a condensed time series with rated power. Partial load charging over multiple hours is then also modeled as partial load, as otherwise the energy procurement would deviate from the actual energy transfer with hourly resolution.

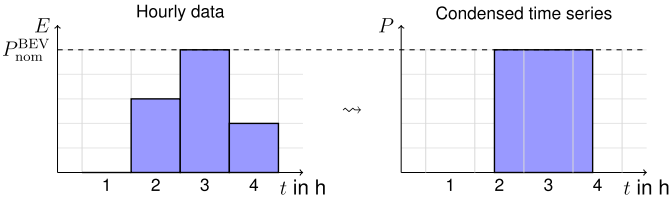

Fig. 6. Transfer of optimized hourly BEV charging profile to continuous time for simulation. The time series is condensed to minimal time with nominal power P_{nom}^{BEV}. The energy content stays the same.

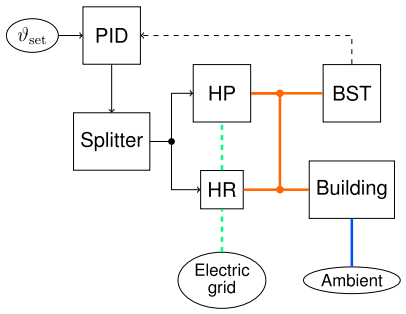

Fig. 7. BHS block diagram. Black lines represent information flows, orange lines represent thermal connections, green dashed lines represent electrical connections, and blue lines correspond to connections under ambient conditions.

3.2.2. Building heating system and disaggregation controller

Decentralized heating systems represent another significant source of flexibility alongside the BEVs considered in this study. In contrast, however, to quantify this flexibility of BHS, it is necessary to consider the BHS in its entirety, as flexibility arises from the interaction of its subcomponents. Low-voltage networks are of particular interest for this study, which is why the modeling of BHS focuses on single-family and multi-family homes. Fig. 7 shows a simplified system diagram of a BHS at this level.[3] This section first provides an overview of the dynamic simulation of the BHS, followed by the aggregation and disaggregation strategies required for the coupling framework.

Dynamic simulation of the BHS. The primary source of heat is the HP, which is supported by a Heater Rod (HR) during colder conditions. In most operating scenarios, the HP alone provides the thermal energy required for space heating. The generated heat flow is then delivered to a busbar that distributes heat to the connected heat sinks. The heat sink is represented by a dynamic building model that utilizes the envelope area method to model residential buildings [19]. This model accounts for the key heat transfer coefficients of the building envelope surfaces to the ambient, as well as thermal masses inside the building.

Part of the BHS are different controller models from which the main model dynamics arise. For the building itself, a temperature controller regulates the heat flow from the heat busbar into the building and therefore regulates the air temperature. The main PID controller regulates the BST temperature based on the setpoint ϑ_{set}^{BST}. In most cases, this setpoint remains constant, as domestic hot water must be supplied at a defined temperature. While some systems use a separate BST for domestic hot water, this model assumes a single-buffer configuration based on a stirred-tank model. Relevant parameters of the BHS model are validated as part of the ERIGrid 2.0 project [1] at the SYSLAB test facility.

Discrete tapping events, representing domestic hot water demand, form an additional sink in the building model. Defined according to European heating system standards, they are characterized by short power peaks that often exceed the heat source capacity, causing the BST to cover the deficit and its SOC to drop temporarily. Unlike the predictable space-heating demand, these non-schedulable loads are particularly relevant for load allocation and are explicitly addressed by the disaggregation controller explained next.

[3] In this study, a typical European heating system was considered. A key characteristic of this system is the hydronic room heating setup, which offers comparatively high flexibility potential arising from the thermal masses of the different components shown in the figure. In other regions, such as North America, heating systems are often based on air heaters, which typically provide lower flexibility potential. Nevertheless, the approach presented in this study is also applicable to these types of systems.

HP aggregation and disaggregation. A higher aggregation level is particularly relevant for complex distributed components such as BHSs, as it enables runtime-efficient analysis of larger energy systems. The central question, however, is to what extent aggregation affects model accuracy and whether the optimization results ensure physical feasibility. This paper, therefore, analyzes the effects of aggregating distributed BHSs, making aggregation and disaggregation integral parts of the coupling framework. The following sections describe this process in detail.

HP aggregation. For model coupling, the simulation results must be transformed both from a continuous-time representation to a temporally discrete resolution and into an aggregated format, i.e., step 3 in Fig. 4. In the optimization of the BHSs, the following model parameters define constraints for the optimization problem and are derived from the simulation output: maximum and minimum storage temperatures, electrical nominal power of the heat sources, and thermal mass of the BSTs. Furthermore, time series of ambient temperature are generated by computing the mean value over each hour. Heating and domestic hot water demands are derived from the corresponding outputs of the simulation model by integrating the respective power over each discrete time interval. To account for component aggregation, these energy demands are summed accordingly.

In the following, we differentiate between three aggregation levels $HP_{(\cdot,1)}$ to $HP_{(\cdot,3)}$. In aggregation level $HP_{(\cdot,1)}$, components are modeled individually, so no dedicated aggregation strategy must be applied. In aggregation level $HP_{(\cdot,2)}$, all components are summed up and treated as one single component. The nominal power of the aggregate corresponds to the sum of the individual nominal powers, and the BST sizes are cumulated accordingly. However, different buildings i typically have different insulation levels and thermal behavior, which motivates the introduction of aggregation level $HP_{(\cdot,3)}$. The building's characteristics are reflected by the effective heat transfer coefficient ϕA_i between ambient and room air and ϕA_i^{indoor} between heating system and room air. These characteristics are used to calculate an individual minimum supply temperature $\vartheta_{i,t}^{BST,\min}$ in (2) to account for ambient temperature dependent heat loss. Therefore, compared to $HP_{(\cdot,2)}$ the constant minimum storage temperature is replaced by a dynamic minimum storage temperature leading to $SOC_{i,t}$ that is dependent on the ambient temperature ϑ_t^{amb}. Based on this, (3) transfers the BST temperature ϑ_i^{BST} to the dynamic SOC.

$$\vartheta_{i,t}^{BST,\min} = \frac{\phi A_i}{\phi A_i^{indoor}} \left(\vartheta_i^{room,nom} - \vartheta_t^{amb}\right) + \vartheta_i^{room,nom} \tag{2}$$

$$SOC_{i,t}(\vartheta^{amb}) = \frac{\vartheta_i^{BST} - \vartheta_{i,t}^{BST,\min}(\vartheta_t^{amb})}{\vartheta_i^{BST,\max} - \vartheta_{i,t}^{BST,\min}(\vartheta_t^{amb})} \tag{3}$$

To accurately capture the efficiency of individual and aggregated HPs, COP data are integrated into the optimization model. For this purpose, an $T \times K$ matrix is constructed based on Eq. (4), where T corresponds to the time steps and K corresponds to SOC steps.

$$COP(SOC) = \eta\left(1 - \frac{\vartheta_t^{amb}}{SOC\,(\vartheta_i^{BST,\max} - \vartheta_{i,t}^{BST,\min}) + \vartheta_{i,t}^{BST,\min}}\right)^{-1}, \eta = 0.40 \tag{4}$$

This matrix enables a discretized representation of different modeling levels:

- $HP_{(2,\cdot)}$ – no temperature dependence: The COP is calculated as the mean value across a matrix row at a fixed nominal SOC as the nominal operating point, and therefore is independent of operating conditions.
- $HP_{(3,\cdot)}$ – ambient temperature dependence: The COP depends on time-discrete ambient temperature. For SOC, the nominal value from $HP_{(2,\cdot)}$ is used.
- $HP_{(4,\cdot)}$ – ambient temperature and SOC dependence: The COP depends on both ambient temperature and SOC, employing the full matrix to account for their combined effects.

At the highest modeling level, $HP_{(5,\cdot)}$, COP values are determined directly within the optimization model, allowing an exact characterization of COP behavior. Therefore, no COP matrix is required for aggregation in the case of $HP_{(5,\cdot)}$.

HP disaggregation. After the optimization, the power values for the BHSs determined by the optimization model must be transferred back into the continuous time domain of the simulation (see step 5 in Fig. 4). Depending on the aggregation level, two distinct approaches can be identified. In case of aggregation level $HP_{(\cdot,1)}$, no disaggregation is needed since components were individually optimized, and therefore, this step can be omitted. In case of $HP_{(\cdot,2)}$ and $HP_{(\cdot,3)}$, the total power of the aggregated BHSs determined by the optimization must be distributed among the individual units during simulation. This task is performed by the newly introduced disaggregation controller. It ensures that the aggregated HP schedule from the optimization is translated into individual setpoints that respect each system's internal state during simulation.

A key aspect of the controller design is to ensure fairness among households. In this study, equity is assumed to be fulfilled when all BSTs have an identical SOC. This ensures that the comfort level of the customers is comparable. This assumption requires that storage sizes are properly dimensioned based on the specific heat demand of each building. For disaggregation, it is essential to ensure that the sensitivity of the SOC to power allocation across individual HPs remains comparable. This condition ensures that power allocations exert a consistent global effect and that, during periods of limited or absent power allocation, SOC losses are of similar magnitude. Therefore, the individual BSTs are designed such that the tank volume V^{BST} is defined by (5)

$$V = \frac{\dot{Q}_{dis}\,\tau^{dis}}{\rho\, c_p\, \Delta T}, \quad \Delta T = 65\ °C - 40\ °C = 25\ °C \tag{5}$$

$$\dot{Q}_{dis} = \phi A(\vartheta^{room,nom} - \vartheta^{amb,nom}), \tag{6}$$

where τ_{dis} is the discharge time, ρ is the density and c_p the specific heat capacity of water, $\vartheta^{room,nom}$ the nominal room temperature, and $\vartheta^{amb,nom}$ the nominal ambient temperature. Calculations show that $\tau^{dis} = 2$ h provides a good reference point for dimensioning. After calculation, the storage volume is mapped to typical commercially available BST sizes.

With this sizing assumption, different HPs can be aggregated, and the disaggregation controller can allocate the power setpoint for each individual HP i from the set of all aggregated HPs H among buildings based on the individual SOC values.

The main operating principle of the disaggregation controller is shown in Fig. 8 and is based on three operational modes:

- *Case 0:* Total available power $P_{tot,t}$ is sufficient to operate all HPs at full load.
- *Case 1:* Total available power is sufficient to cover the sum of minimum load $P_{min,i}$ with $i \in H$.
- *Case 2:* Total available power is insufficient to meet the minimum load requirements of all HPs.

In *Case 0*, the allocation is straightforward. All HPs can operate at full load $P_{max,i}$, and the total available power is distributed proportionally to the nominal electrical power of each unit.

In *Case 1*, the minimum operation level is ensured for all HPs. The remaining power (i.e., $P_{tot} - \sum_i P_{min,i}$) is distributed using a scaling factor (k_i) defined in (7). This allows prioritization based on SOC differences, ensuring a non-linear weighting toward lower SOC values. To ensure sensitivity in lower scales, an exponent of 10 was derived by empirical tests.

$$k_i = \frac{(1 - SOC_i)^{10}}{\sum_j (1 - SOC_j)^{10}} \tag{7}$$

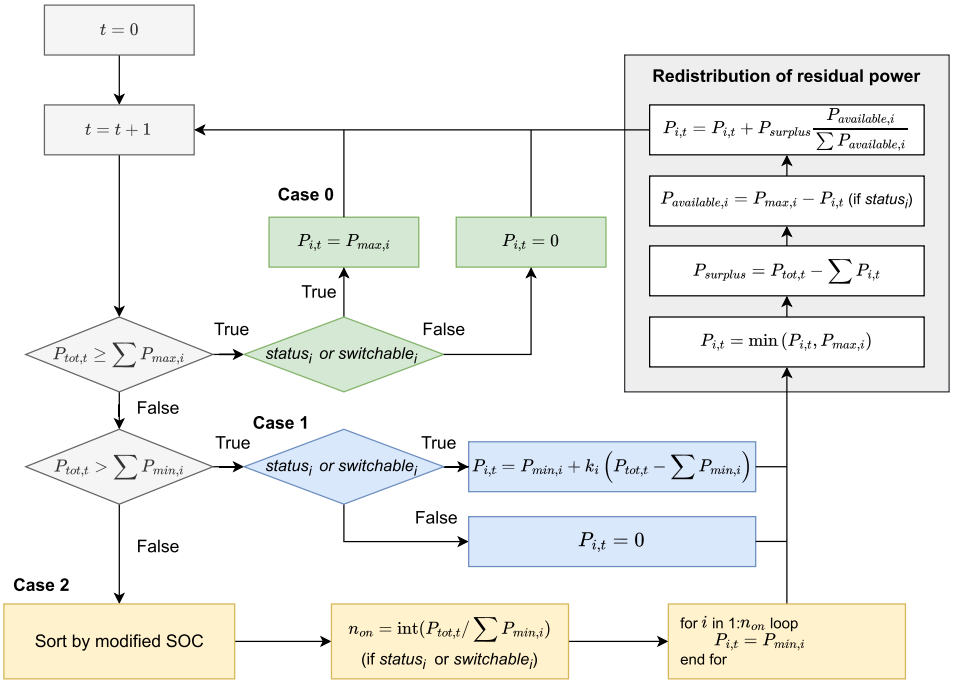

Fig. 8. Schematic flowchart illustrating the sequence of operations in the disaggregation controller (where i denotes the index of the heat pump and t the time step). All expressions denote assignments and are intended as pseudo-code.

Furthermore, the operational status of each HP is considered, as real-world systems include minimum up- and downtime requirements. Each unit tracks an internal *status* and *switchable* state, which determine whether the HP is currently running or eligible to be turned on. Only those HPs that are switched on or able to switch operational state receive an allocation based on their minimum load and scaling factor. If a HP is unavailable, it receives no power. The surplus power ($P_{surplus}$) is then redistributed among the remaining available HPs according to their unused power capacity ($P_{available}$) based on the assignment function in (8).

$$P_{i,t} = P_{i,t} + P_{surplus} \frac{P_{available,i}}{\sum_i P_{available,i}}. \tag{8}$$

In *Case 2*, some HPs must be deactivated because the total available power cannot satisfy the aggregate minimum demand. In this case, HPs are prioritized based on their SOC, with those having the lowest SOC selected first. As many HPs as possible are supplied at their minimum load (P_{min}). Finally, any remaining power is distributed among the active units in the same way as described in Case 1.

Special attention is required when the SOC reaches its lower temperature limit while heating demand is high due to low ambient temperatures. In such cases, the available thermal output decreases with declining SOC, which may prevent the building from maintaining the target room temperature. To address this, aggregation level $HP_{(\cdot,3)}$ employs a modified SOC that incorporates a building-specific minimum supply temperature $T_{min,i,dyn}$ that is calculated by the ambient temperature specific heating demand. At low ambient temperatures, the minimum storage temperature increases and the calculated SOC decreases accordingly, prompting the disaggregation controller to allocate additional power to affected buildings. This approach supports the fairness objective of the developed disaggregation controller. The modified SOC is evaluated according to Eq. (3). The definition of a dynamic SOC allows individual contractual agreements for defining comfort levels to be taken into account. While this may be common in real-world applications, this study assumes identical comfort conditions for all households, as the underlying methodology remains unaffected by this assumption.

This enables the controller to better account for building insulation levels and to distribute the resulting household energy demands fairly. A drawback of this approach is the high degree of data availability for the aggregator, as individual building parameters must be known. In this study, however, it is assumed that such data can be made available within the framework of the EEBUS[4] standard and communicated via the smart meter gateway.

3.3. Dynamic simulation and market optimization – an interface

A physically consistent exchange of information between the dynamic simulation and the market optimization requires an explicit interface that translates continuous-time trajectories into discrete optimization intervals and vice versa. In the presented framework, this applies in particular to steps 3 and 5, where simulation outputs are preprocessed for optimization and the resulting setpoints are subsequently transferred back into the simulation environment.

A central task of the interface is to reconcile different temporal representations. Dynamic simulations typically operate on an irregular, solver-dependent time grid with variable step sizes, while the market optimization requires uniformly sampled signals, usually at an hourly resolution for day-ahead scheduling. Therefore, simulation data must be resampled appropriately.

For *state variables* such as temperature ϑ, the value at a given sampling instant depends only on the instantaneous state. Consequently, resampling is performed by linear interpolation between the two simulation points surrounding the sampling time.

For *process variables* such as heat flow rate $\dot{Q}$, however, the entire trajectory between two sampling points is physically relevant [24]. In this case, the quantity of interest is the integral of the process variable over time. The interface therefore first computes the cumulative integral by applying the trapezoidal rule,

$$I_i = \sum_{k=0}^{i-1} \frac{y_k + y_{k+1}}{2} (x_{k+1} - x_k), \tag{9}$$

[4] EEBUS is a Europe-based communication standard that enables interoperable energy management between household devices, energy systems, and the power grid.

followed by linear interpolation of the integrated trajectory, denoted I^{int}, using the same interpolation scheme as for state variables. The resampled process variable is then obtained by numerical differentiation,

$$y^{\text{int}}(t_i) = \frac{I^{\text{int}}(t_i) - I^{\text{int}}(t_{i-1})}{t_i - t_{i-1}}. \tag{10}$$

In the next section, the different optimization models are explained in more detail.

3.4. Comparative flexibility representations across component modeling depths

The preceding sections introduce a physics-based simulation model that captures component behavior in detail. This engineering perspective enables both stand-alone simulations of component dynamics and the calculation of system states based on external inputs. Optimization provides the link between the two, aligning flexibility with price signals. This section details technology-dependent flexibility constraints in market-oriented optimization models across component modeling depths identified by the classification framework in Section 2.1.

3.4.1. BEV representation

The basic $\text{BEV}_{(1,\cdot)}$ model comprises charging and capacity constraints, considering availability (11), charging efficiency and battery state (12), (13), as well as capacity (14):

$$0 \leq P_{v,t}^{BEV} \leq p_v^{BEV,nom} \cdot avail_{v,t} \quad : \forall v,t \tag{11}$$

$$STO_{v,t}^{BEV} = STO_{v,t-1}^{BEV} + (\eta_v^{BEV} \cdot P_{v,t}^{BEV} - dem_{v,t}^{bev}) \cdot \Delta t \quad : \forall v,t \tag{12}$$

$$STO_{v,0}^{BEV} = sto_v^{BEV,init} \quad : \forall v \tag{13}$$

$$0 \leq STO_{v,t}^{BEV} \leq cap_v^{BEV} \quad : \forall v,t \tag{14}$$

To enhance realism, $\text{BEV}_{(2,\cdot)}$ expands the model by implementing a minimum charging current ($p^{BEV,\min}$) in (15). The extension utilizes a Big-M formulation (16) and binary auxiliary variables (17) to indicate whether a BEV is actively charging:

$$p^{BEV,\min} \cdot B_{v,t} \leq P_{v,t}^{BEV} \quad : \forall v,t \tag{15}$$

$$P_{v,t}^{BEV} \leq m^{BEV} \cdot B_{v,t} \quad : \forall v,t \tag{16}$$

$$B_{v,t} \in \{0,1\} \quad : \forall v,t \tag{17}$$

Further physical detail is incorporated in $\text{BEV}_{(3,\cdot)}$ by considering the endogenous power losses of on-board systems ($p_v^{BEV,ob}$) during charging. In accordance to Eqs. (1), (12) is replaced by the updated Eq. (18):

$$STO_{v,t}^{BEV} = STO_{v,t-1}^{BEV} + \left(\eta_v^{BEV} \cdot P_{v,t}^{BEV} - B_{v,t} \cdot p_v^{BEV,ob} - dem_{v,t}^{BEV}\right) \cdot \Delta t \quad : \forall v,t \tag{18}$$

Table 2 provides an overview of the model classifications regarding operations-research related characteristics.

Table 2
Overview of BEV models. The class of the models assumes a linear objective function.

	$\text{BEV}_{(1,\cdot)}$	$\text{BEV}_{(2,\cdot)}$	$\text{BEV}_{(3,\cdot)}$
Class	LP	MILP	MILP
# linear constraints	$3 \cdot \lvert V\rvert \cdot \lvert T\rvert$	$5 \cdot \lvert V\rvert \cdot \lvert T\rvert$	$6 \cdot \lvert V\rvert \cdot \lvert T\rvert$
# quadratic constraints	–	–	–
# continuous variables	$2 \cdot \lvert V\rvert \cdot \lvert T\rvert$	$2 \cdot \lvert V\rvert \cdot \lvert T\rvert$	$2 \cdot \lvert V\rvert \cdot \lvert T\rvert$
# binary variables	–	$\lvert V\rvert \cdot \lvert T\rvert$	$\lvert V\rvert \cdot \lvert T\rvert$
Relevant constraint groups	(11)–(14)	(11)–(17)	(11), (13)–(18)

3.4.2. HP representation

With the most basic HP formulation $\text{HP}_{(1,\cdot)}$, the temperature of the heat storage is not explicitly tracked. Instead, the integral of the consumed power P_t^{HP} has to maintain a certain level throughout the planning horizon (19). Given a normative demand profile ($p_t^{HP,dem}$), the bounds (ε_t) of the integral account for the flexibility inherent to the BHS. For a more detailed description refer to [13]. Furthermore, constraints (20) ensure that the electrical power consumption of the HP stays within given limits. For the sake of brevity, formulations are given for a single HP or aggregate:

$$-\varepsilon_t \leq \sum_{\hat{t} \leq t} (p_{\hat{t}}^{HP,dem} - P_{\hat{t}}^{HP}) \leq \varepsilon_t \quad : \forall t \tag{19}$$

$$0 \leq P_t^{HP} \leq p^{HP,nom} \quad : \forall t \tag{20}$$

More detailed model formulations explicitly couple HP operation and BST charging via different representations of the COP. COP-related values correspond to the dynamic simulation provided by Eq. (4) or its discretizations, dependent on the modeled case.

Model formulations of category $\text{HP}_{(2,\cdot)}$ and $\text{HP}_{(3,\cdot)}$ assume a COP depending on the ambient temperature, disregarding the dependency on the supply temperature (i.e., the BST's temperature):

$$SOC_t = SOC_{t-1} + (Q_t - dem_t^{HP}) \cdot \Delta t \cdot conv \quad : \forall t \tag{21}$$

$$\vartheta_t^{BST,\min} \leq SOC_t \leq \vartheta^{BST,\max} \quad : \forall t \tag{22}$$

$$SOC_0 = \vartheta^{BST,init} \tag{23}$$

$$SOC_{t^{max}} \geq \vartheta^{BST,init} \tag{24}$$

$$Q_t = cop_t \cdot P_t^{HP} \quad : \forall t \tag{25}$$

(20)

Eq. (21) tracks the temperature in the BST. The thermal power provided by the HP (Q_t) and the heat demand (dem_t^{HP}) in time step t with duration Δt are taken into account. The impact of the resulting heat flow on the SOC is calculated using a conversion factor $conv$. This factor can be calculated as follows:

$$conv = (mass \cdot c_p)^{-1},$$

with $mass$ being the mass of the BST and c_p the specific heat capacity of the storage medium. Constraints (22) prevent cooling down and overheating of the BST, while (23) and (24) define the initial and final SOC. Lower temperature limits of the BST can be time-dependent, as cooler periods may only allow a higher minimum temperature to supply enough thermal energy for room heating (see Section 3.2.2). Electrical power consumption and thermal power supply of the HP are linked in (25). The difference between $\text{HP}_{(2,\cdot)}$ and $\text{HP}_{(3,\cdot)}$ lies within the parametrization of cop_t. For category $\text{HP}_{(3,\cdot)}$, the COP is specified individually for each time step, while models of category $\text{HP}_{(2,\cdot)}$ use a constant value over all time steps. Power limits still apply.

Models of category $\text{HP}_{(4,\cdot)}$ incorporate approximations of the COP that is dependent on the BST's temperature. While the formulations of $\text{HP}_{(2,\cdot)}$ and $\text{HP}_{(3,\cdot)}$ are straightforward and uniform, there exist multiple different formulations to approximate endogenous COP operation within an optimization model. In the reviewed literature, for category $\text{HP}_{(4,\cdot)}$, the COP is mostly modeled as a variable itself. Regarding the relation between COP, thermal and electrical power (see (25)), the formulation would either become quadratic or is linearized. An example of each, quadratic and linearized models, is presented in [32].

In the formulation presented below, a step function is used to approximate the COP model endogenously. The range of the possible SOC is discretized into sections. For each section, a constant COP is assumed. See Fig. 9 for a visual representation. Binary variables $Z_{k,t}$ are introduced to indicate whether the SOC of given time step t lies within section

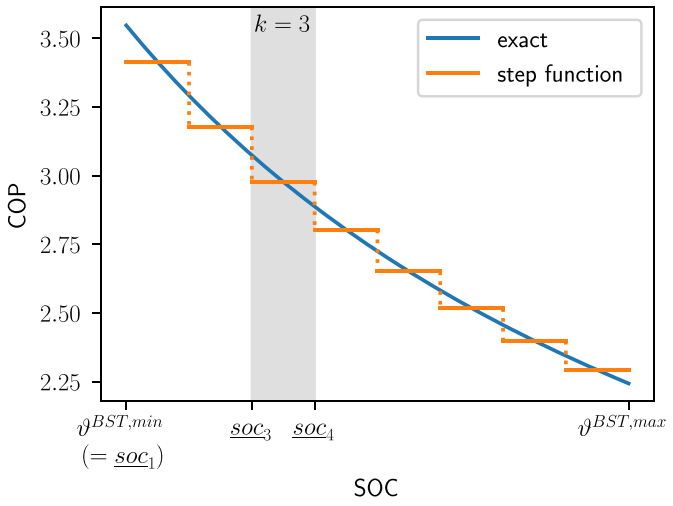

Fig. 9. Stepwise approximation of COP with $|K| = 8$ steps for a single time step.

k (26), (27). Additionally, the power consumption of the HP is modeled for each section and time step individually:

$$\underline{soc}_{k,t} \cdot Z_{k,t} \leq SOC_t \quad : \forall k,t \tag{26}$$

$$SOC_t \leq \underline{soc}_{k+1,t} + m^{HP} \cdot (1 - Z_{k,t}) \quad : \forall k \neq k^{max}, t \tag{27}$$

$$\sum_k Z_{k,t} = 1 \quad : \forall t \tag{28}$$

$$0 \leq P^{HP}_{k,t} \leq p^{HP,nom} \cdot Z_{k,t} \quad : \forall k,t \tag{29}$$

$$Q_t = \sum_k (cop_{k,t} \cdot P^{HP}_{k,t}) \quad : \forall t \tag{30}$$

$$Z_{k,t} \in \{0,1\} \quad : \forall k,t \tag{31}$$

(21), (22), (23), (24)

If the SOC is within the interval $[\underline{soc}_k, \underline{soc}_{k+1}]$, $Z_{k,t}$ can assume the value 1 and if so, section k is referred to as "active", while this can only be true for one section (28). Note that in edge cases where $SOC = \underline{soc}_k$, either adjacent section $k-1$ or k can be set to be active. When minimizing procurement costs, usually the one corresponding to the more efficient COP is chosen. If a section is active, the corresponding power may not exceed the HP's limit. If it is not active, any power consumption is restricted for this section (29). Since only one section can be active, the overall power consumption of the HP is equivalent to the active section's power consumption. Analogously to $HP_{(2,\cdot)}$ and $HP_{(3,\cdot)}$, (30) defines the heat provided by the HP. As the COPs are parametric inputs for the optimization, there is no need for linearization. However, through the introduction of binary variables (31) the model is a mixed-integer linear program. The HP operation's impact on the SOC and its constraints are considered in the same way as for $HP_{(2,\cdot)}$ and $HP_{(3,\cdot)}$.

There is no need for an approximation of the COP if the model is allowed to be non-linear. Models with these properties are categorized in $HP_{(5,\cdot)}$. An exact calculation of the COP can be incorporated in the optimization with the following formulation:

$$COP^{QP}_t = \eta^{HP} \cdot \frac{SOC_t}{SOC_t - \vartheta^{amb}_t} \quad : \forall t \tag{32}$$

$$Q_t = COP^{QP}_t \cdot P^{HP}_t \quad : \forall t \tag{33}$$

(20), (21), (22), (23), (24)

Here, (32) is the Carnot COP corrected by an efficiency factor η^{HP} with ϑ^{amb} being the temperature of the heat source. Eq. (33) links heat flow and electrical power analogous to (25), and (30). However, since COP^{QP} is now also a variable, (33) is quadratic—as is (32), when rearranged. (20)-(24) apply as before. Table 3 provides an overview of the different model formulations regarding model characteristics and problem size.

Table 3
Overview of HP models. The class of the models assumes a linear objective function.

	$HP_{(1,\cdot)}$	$HP_{(2/3,\cdot)}$	$HP_{(4,\cdot)}$	$HP_{(5,\cdot)}$
Class	LP	LP	MILP	QCP
# linear constraints	$2 \cdot \lvert T \rvert$	$4 \cdot \lvert T \rvert$	$4 \cdot \lvert T \rvert + 4 \cdot \lvert T \rvert \cdot \lvert K \rvert$	$3 \cdot \lvert T \rvert$
# quadratic constraints	–	–	–	$2 \cdot \lvert T \rvert$
# continuous variables	$\lvert T \rvert$	$3 \cdot \lvert T \rvert$	$2 \cdot \lvert T \rvert + \lvert T \rvert \cdot \lvert K \rvert$	$4 \cdot \lvert T \rvert$
# binary variables	–	–	$\lvert T \rvert \cdot \lvert K \rvert$	–
Relevant constraint groups	(19), (20)	(20)–(25)	(21)–(24), (26)–(31)	(20)–(24), (32), (33)

Table 4
Aggregator related techno-economic configuration parameters. Electrical power, BST mass, storage capacity, and consumption range are provided for a component level. Average consumptions refer to the customer baseline load.

HPs	BEVs
nb. of components $\lvert H \rvert = 104$	nb. of components $\lvert V \rvert = 149$
el. power = 1.35 – 7.38 kW	nb. of models = 4
BST mass = 300 – 1500 kg	el. power = 7.2 – 22 kW
$\varnothing_t$ therm. consumption = 672.68 kW	capacity = 52 – 82 kWh
	$\varnothing_t$ el. consumption = 45.21 kW

4. Case study

4.1. Aggregator modeling and decision-relevant influences

A case study on energy procurement is being conducted to investigate the representation of physical effects in cost-oriented optimization models. The engineering-oriented simulation transitions from active internal control to price-driven operation to benchmark the optimization results regarding physical detail. Specifically, an aggregator of flexible loads is considered, and an objective function (Eq. 34) is incorporated into the techno-economic constraints to minimize operation costs of $BEV_{(n,m)}$ and $HP_{(n,m)}$ models, which differ in physical depth.

$$\min \quad C^{agg} = \sum_t \left(\left(\sum_v P^{BEV}_{v,t} + \sum_h P^{HP}_{h,t} \right) \cdot \pi_t \right) \tag{34}$$

where π_t corresponds to electricity prices, $v \in V$ and $h \in H$ to vehicles and heat pumps, respectively.[5] The administrative area of the aggregator comprises a distribution grid with 104 households based on the SimBench grid *1-LV-semiurb5–0-no_sw* ([34]). Table 4 displays the techno-economic system configuration.

The model horizon spans one week. Consequently, historic weather data ([43]) (see *Step 1 - Scenario Data* in Fig. 4,) and historic day-ahead prices ([2]) (see π_t in eq. (34)) are utilized for the dynamic simulation and the optimization model, respectively.[6] The historical week considered for parameterization of both models is from January 8th, 2024, to January 15th, 2024. It shows significant variance in ambient temperatures (German average, ranging from −7 °C to +5 °C) and day-ahead prices (German market zone, ranging from 6 ct/kWh to 15 ct/kWh).

The modeling of BEVs requires driving profiles that specify charging availability and trip energy consumption. The driving profiles are derived from a study on individual mobility patterns [39]. The dataset

[5] If heat pumps are aggregated, $|H| = 1$.

[6] Note that explicit retail prices include additional fees, not affecting optimization outcomes due to their static nature.

serves as the basis for a stochastic profile generator. Two sequential random draws determine departure and return times as well as the driven distance of each BEV, resulting in individually different profiles [56]. Parameters that determine energy consumption during driving are provided in the form of BEV model-specific nominal consumption data.

Building model parameters are based on current residential construction standards. Specifically, the German Building Energy Act (GEG) [14] provides thermal insulation requirements for new buildings, while DIN EN 12,831 [19] provides representative values for the existing building stock. To create a diverse building portfolio, both parameter sets are blended linearly using a uniformly distributed random number for each envelope component. The resulting heat transfer coefficient is computed according to (35) where ϕ_e^{BEA} is the heat transfer coefficient described in the Building Energy Act, ϕ_e^{DIN} is the same value in the DIN EN 12831, both for the envelope type e with E as set of walls, windows, floor and ceiling, and u as a random number calculated for each building.

$$\phi A = \sum_{e \in E} A_e \left(u\, \phi_e^{BEA} + (1-u)\, \phi_e^{DIN} \right), \quad u \in [0;1] \tag{35}$$

The respective areas A_e required for the envelope model are determined based on typical building area ratios, derived from values provided in DIN EN 17,037. To ensure that a representative building stock is represented in this study, meta-information on various buildings is taken from a benchmark network model from the SimBench dataset for low voltage [33]. The building size is scaled by the yearly energy consumption given in the scenario description.

4.2. Scenario selection

The scenario analysis conducts the full BEV component range ($\mathrm{BEV}_{(1,\cdot)}$-$\mathrm{BEV}_{(3,\cdot)}$) on a single component modeling level ($\mathrm{BEV}_{(\cdot,1)}$). To maintain the focus on the identified research gap (see Section 2.2), the case study excludes BEV aggregation, which was previously examined by [38]. However, because of their continual availability and high level of simultaneous operation, aggregating HPs offers a promising way to simplify single-component modeling approaches. Thus, the analysis comprises all three identified HP aggregation levels, ranging from single-component modeling ($\mathrm{HP}_{(\cdot,1)}$) to insulation dependent aggregation ($\mathrm{HP}_{(\cdot,3)}$). In terms of component modeling depth, $\mathrm{HP}_{(1,\cdot)}$ and $\mathrm{HP}_{(2,\cdot)}$ differ only in parametrization, despite having different formulations. Thus, the study excludes $\mathrm{HP}_{(1,\cdot)}$ and focuses on $\mathrm{HP}_{(2,\cdot)}$ to $\mathrm{HP}_{(5,\cdot)}$.

All approaches considered in the scenario analysis are analyzed with respect to their results regarding techno-economic optimization, physical validity, and optimization runtime.

5. Results

Optimizing sector coupling technologies primarily aims to minimize techno-economic values, such as costs, demands, or emissions. However, modelers must weigh up corresponding (i) objective-related values with (ii) the feasibility of optimized dispatch decisions in real-world applications and (iii) model complexity. To quantify these trade-offs, this section analyses the implications of using different optimization model formulations introduced in Section 3, while keeping the underlying dynamic simulation model fixed. In other words, only the mathematical representation within the optimization domain is varied, allowing a direct assessment of how modeling depth and aggregation affect techno-economic results (Section 5.1), physical validity (Section 5.2), and computational performance (Section 5.3).

5.1. Optimization: techno-economic results

Dependencies between the illustrations of physical relationships in optimization models directly result in variations of their solution space and techno-economic interactions. These variations affect key parameters such as energy demands or objective values. The case study's optimization results are analyzed firstly regarding different component modeling depths, followed by an analysis regarding aggregation level assumptions, both ranging through the predefined scenario selection described in Section 4.2. Physical validation or realism and corresponding simulation results are excluded here and are particularly examined in Section 5.2.

Component modeling depth. While Fig. 10(a) shows corresponding techno-economic key parameters for various BEV modeling approaches, Fig. 10(b) provides results of HP models. Increasing the level of physical detail in BEV dispatch introduces additional constraints, potentially reducing the solution space, and accounts for endogenous charging inefficiencies. Consequently, energy demand and associated procurement costs increase with the hierarchical component modeling depth. Overall, we observe a maximum underestimation of approximately 3% in demand and costs when employing the lowest modeling depth. This translates to approximately €20 in total costs for the aggregated fleet (149 BEVs) for the full model horizon (one week). While this deviation

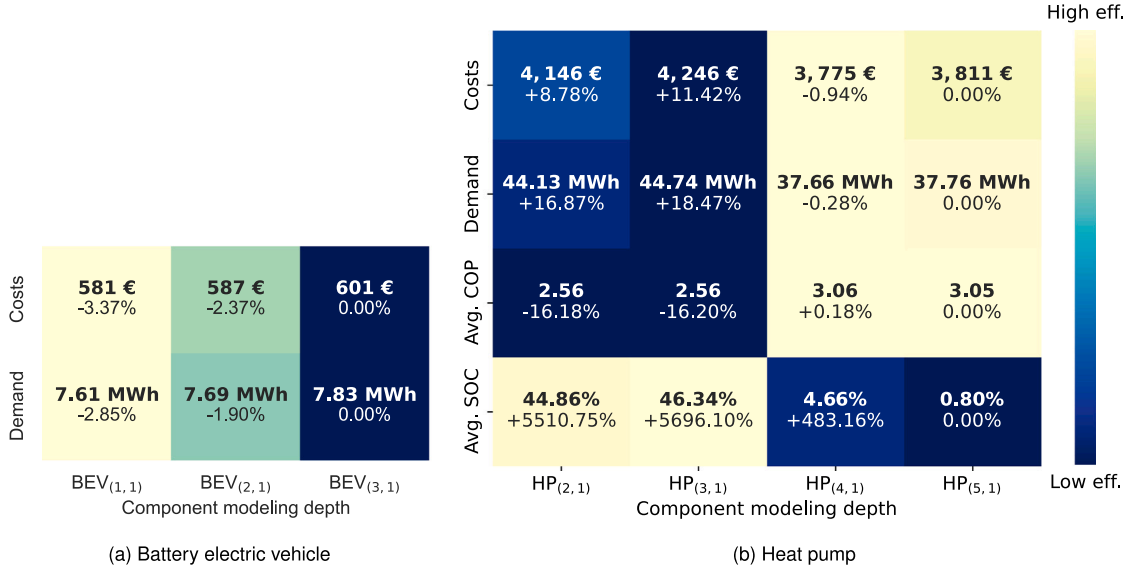

Fig. 10. Techno-economic results showing absolute values for different component modeling depths and percentage deviation in relation to the highest level. The color scheme indicates techno-economic efficiency but does not imply validation or realism.

may be negligible for individual end-users, it can be significant for aggregators managing large fleets of BEVs with substantial charging costs. For instance, the British aggregator *Octopus Energy*, which optimizes approximately 150,000 BEVs solely in the UK, would underestimate the total charging costs by approximately €20,000 per week or about €1,000,000 per year, assuming similar wholesale price patterns.

Considering HPs, the exogenous COP approaches ($HP_{(2,\cdot)}$ and $HP_{(3,\cdot)}$) are distinguishable between ambient temperature dependencies: $HP_{(2,\cdot)}$ assumes a flat COP, while the one of $HP_{(3,\cdot)}$ drops when ambient temperature is low, i.e., when there is increased heat demand. In consequence, $HP_{(2,\cdot)}$ underestimates energy demand and related costs slightly. The main driver regarding key techno-economic parameters is whether the COP is modeled exogenously or endogenously. Exogenous approaches optimize flexibility solely based on electricity prices, utilizing the full range of the SOC, resulting in an average SOC of approximately 45–46%. In contrast, endogenous COP approaches ($HP_{(4,\cdot)}$ and $HP_{(5,\cdot)}$) lower procurement costs by about 9–11% by reducing electricity demand through lower buffer storage temperatures, which yield higher COP values (about 16%). In $HP_{(5,\cdot)}$, almost the complete flexibility is used to leverage such SOC-COP dependencies, resulting in an average SOC of less than 1%. In conclusion, the price gradient is often insufficient to offset the opportunity costs associated with a reduced COP, and price variations are not capitalized on. This suggests that, from a consumer's perspective, COP optimization may be more effective than leveraging flexibility for system efficiency in electricity market models, potentially overestimating the benefits of demand response mechanisms. However, given the dynamics of SOC-COP relations, the utilization of flexibility is found to be contingent upon price gradients and ambient temperatures.

When approximating the endogenous SOC-COP relationship ($HP_{(4,\cdot)}$), the cost difference relative to the exact COP formulation ($HP_{(5,\cdot)}$) remains small (around −1%). This underestimation of demand and costs in $HP_{(4,\cdot)}$ stems directly from the model simplification of discretizing the SOC: Assuming a discretized SOC with 11 equidistant steps allows the buffer storage tank to be filled to nearly 10% without impacting the COP (see Fig. 9). Consequently, $HP_{(4,\cdot)}$ may optimize against energy price variations to a certain extent, but does not fully account for COP-related opportunity costs. This results in an average SOC of about 5%, five times higher than that of $HP_{(5,\cdot)}$, while maintaining a similar COP.

Aggregation level. Fig. 11 presents KPI deviations between the optimization results regarding different aggregation levels ($HP_{(\cdot,2)}$ and $HP_{(\cdot,3)}$) compared to single-component modeling ($HP_{(\cdot,1)}$). For costs and demands, the maximum mean absolute percentage error (MAPE) due to aggregation is negligible, remaining below 0.3%. This clearly shows that aggregating HPs does not lead to the feared problem of overestimating flexibility potentials regarding techno-economic objectives, such as cost minimization. In comparison to Fig. 10, the conclusion from a techno-economic modeling perspective is to focus on component modeling depth first, and aggregation level second when modeling HPs.

Regarding Fig. 11(a), the results indicate that increasing the component-level of physical detail in the optimization model leads to higher aggregation errors, highlighting the importance of employing a higher aggregation level for $HP_{(4,\cdot)}$. A comparison of Fig. 11(a) and 11(b) demonstrates that errors decrease with increasing aggregation level slightly, as $HP_{(\cdot,3)}$ reflects more building-specific physics.

5.2. Physical validity of the optimization results

While Section 5.1 analyzed the techno-economic implications of different modeling depths and aggregation levels, the following section examines their physical feasibility within the established coupling framework. To this end, dynamic simulation is deliberately employed as an integral part of the analysis strategy, enabling a systematic evaluation of how accurately the market-oriented optimization reproduces realistic component behavior. The objective is to identify the errors that occur at different modeling depths and to quantify their influence on the physical system response, resulting in a comparative assessment of model accuracy across all formulations.

For this purpose, the optimized operating schedules are applied to the component models according to steps 5 and 6 of the coupling framework (see Fig. 4), beginning with the BEV results and followed by the HP results.

5.2.1. Results on battery electric vehicles

Fig. 12 compares the different component modeling depths. The simulation covers 976 charging events over one week. As performance metric serves the SOC difference and is expressed as a histogram. Positive values indicate that less energy was procured than required to reach the target SOC, implying an overestimation of efficiency. Conversely, negative values indicate an underestimation of efficiency. An ideal model yields a difference of zero. The distribution results from comparing the expected and simulated SOC after each charging event.

Fig. 12(a) applies the dispatch function *direct mapping* explained in Section 3.2.1, where the optimization results are imposed directly on the components without modification (see Fig. 6, left). In mode $BEV_{(1,\cdot)}$, the distribution appears broader and flatter, indicating comparatively large deviations. This behavior results from the inaccurate representation of the on-board charger efficiency. In contrast, modes $BEV_{(2,\cdot)}$ and

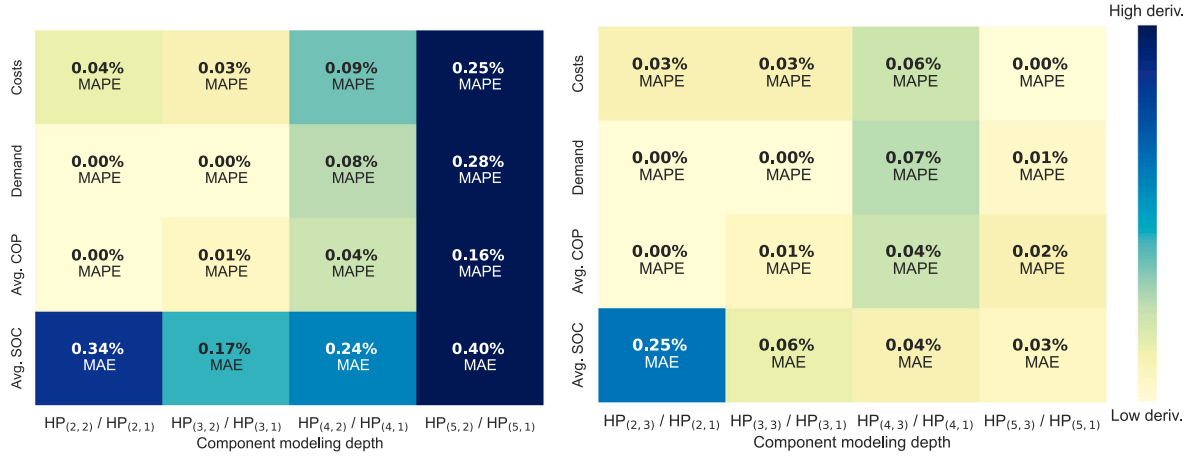

Fig. 11. Deviation between HP aggregation levels compared to single-component modeling. The color scheme indicates aggregation errors for each metric.

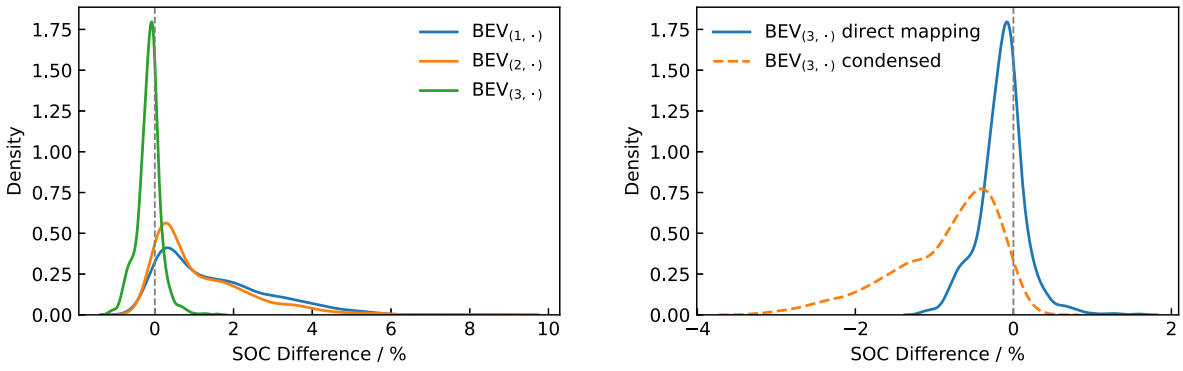

(a) Different component modeling depths. (b) Different dispatch modes

Fig. 12. Comparison of the BEV SOC differences between optimized and simulated results.

$BEV_{(3,\cdot)}$ yield narrower distributions concentrated around zero, reflecting a closer match to the actual efficiency. Among these, $BEV_{(3,\cdot)}$ achieves the best overall approximation.

Fig. 12(b) compares the different dispatch modes. The *direct mapping* mode yields lower deviations than the *condensed* mode. In the latter, the optimized load profile is modified. While the optimized hourly energy purchase from the grid is preserved, the *condensed* mode representation of the load profile leads to a less accurate prediction of efficiency. This results in systematically larger deviations. To avoid these discrepancies, it is necessary to increase the temporal resolution of the optimization model. However, this conflicts with the typical trading intervals in the wholesale electricity market. A reformulation of the optimization model could provide a remedy by applying a finer resolution of the BEV efficiency curve. This approach would require either a linearization of the model or a non-linear formulation. This study does not pursue this aspect further.

It can further be observed that even with the most detailed component modeling, $BEV_{(3,\cdot)}$ still exhibits relatively large deviations. The underlying reason lies in the approximation of the efficiency curve based on the measurements shown in Fig. 5. The applied model proves to be less suitable for certain BEV types. Since in this case the deviations accumulate over time, the discrepancy between charging events increases with a longer time horizon.

Fig. 13 shows the overall charging efficiencies for the BEVs. In *direct mapping* mode, slight differences occur, whereas in *condensed* mode the efficiency remains constant due to fixed charging speed at nominal power. On average, in *condensed* mode the efficiency is 2.4% higher.

5.2.2. Heat pump specific results

To analyze the impact of different modeling depths of the HPs, a dynamic simulation is carried out in analogy to the BEVs. As in the previous case, the internal controllers of the BHS are disabled, and the power set-points obtained from the optimization are directly applied to the individual components. In addition to the analysis of modeling depth, the level of aggregation is also examined. In the component-level modeling, the HPs directly receive the optimized set-points, also bypassing the controllers, since the optimization is performed at the unit level. In the aggregated modeling, the previously described disaggregation controller is used to distribute the centralized set-point among the individual components.

Fig. 14 first compares the COP for different component modeling depths. As evaluation metrics, both the RMSE and the MAE of the difference between optimized and simulated COP are considered. Both indices are unnormalized, i.e., expressed in the numerical range of the COP. It can be observed that there is no significant difference between $HP_{(2,\cdot)}$ and $HP_{(3,\cdot)}$ in terms of COP accuracy, although $HP_{(3,\cdot)}$ performs slightly better. The aggregation level makes no difference in this case. A clear difference appears when moving from the static COP model to the SOC-dependent COP model. At $HP_{(4,\cdot)}$, the average deviation in COP is reduced by approximately 83%. This improvement is attributable to the endogenous calculation of the COP. The aggregation level has no discernible influence. Overall, the RMSE, which disproportionately weights higher deviations, yields a result comparable to the MAE. Fig. 15 illustrates the optimized and simulated COP values for the different component modeling depths in a diagram over time. Despite the reduced fluctuations over time, with higher component modeling depths, the reduced error is discernible.

In addition to COP, the energy balance represents another relevant metric for comparing results. In Fig. 16, the absolute integral of the optimized heat flow is related to the total simulated energy turnover. The results show a pattern analogous to COP: with increasing model accuracy, the energy deviation decreases. However, the comparison between $HP_{(4,\cdot)}$ and $HP_{(5,\cdot)}$ reveals a more pronounced difference. This discrepancy can be explained by the dynamics of operating-point shifts in the BHS. In $HP_{(4,\cdot)}$, the discretized COP estimation used in the optimization creates SOC intervals with identical COP values. More minor price fluctuations therefore provide additional optimization potential for the aggregator, as SOC shifts, and the associated use of component

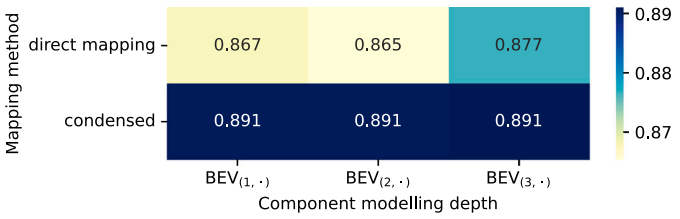

Fig. 13. Different charging efficiencies summarized over all charging events of the BEVs for various component modeling depths.

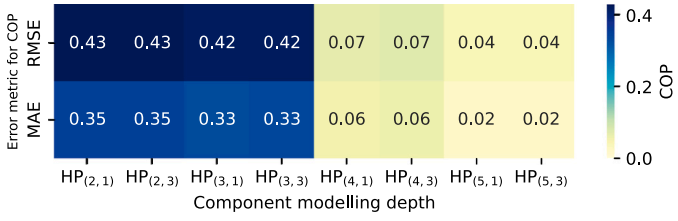

Fig. 14. COP error metrics for different component modeling depths at HP between optimization and simulation.

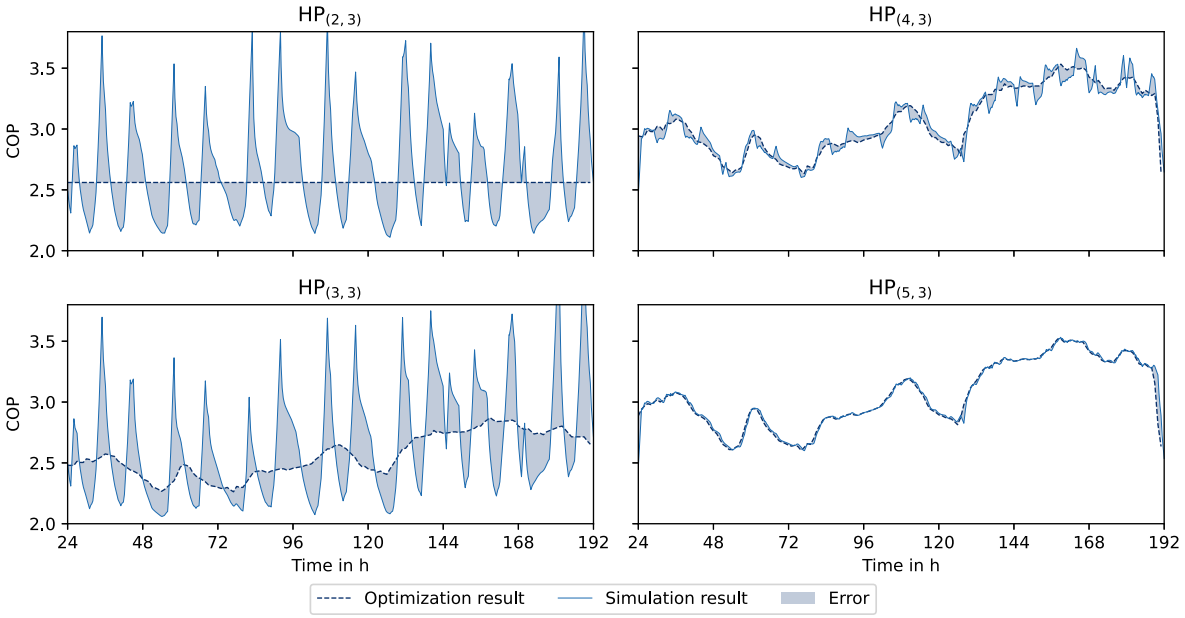

Fig. 15. Comparison of the optimized and simulated COP for the different component modeling depths.

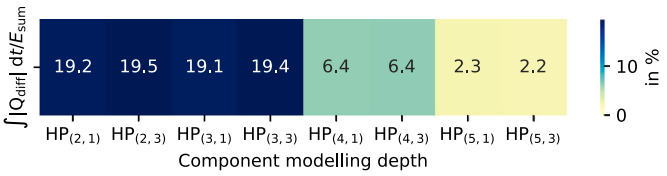

Fig. 16. Thermal turnover for different component modeling depths at HP.

flexibility, within a discretization step entails no efficiency losses. The resulting higher volatility leads to larger deviations in $HP_{(4,\cdot)}$. At $HP_{(5,\cdot)}$, this effect is much less pronounced, as even small SOC fluctuations already lead to COP deviations. Here, too, the influence of aggregation remains negligible.

Fig. 17 illustrates the temporal evolution of the optimized and simulated heat flow rate. At low component modeling depth, not only stronger fluctuations but also large deviations become apparent, which can be directly attributed to inaccurate COP calculations. In the second half of the simulation period, deviations are particularly pronounced after extended system operation. This behavior results from underestimation of the COP, leading to excess heat production that cannot be stored due to elevated system temperatures. In such cases, the simulation model overrides the optimization output, producing larger deficits accompanied by a self-regulation effect.

Finally, room temperature is examined, as this metric is directly relevant for end users. Fig. 18 shows the minimum room temperatureas deviation from the set-point observed during the study period, providing a fair assessment of performance under low ambient temperatures. To account for short domestic hot-water tapping events, which cause brief load peaks that cannot be anticipated in the hourly optimization due to its coarse temporal resolution, two additional optimization runs were conducted with increased lower SOC bounds of 10% and 20%. The results show that higher model accuracy enables better maintenance of room temperature, even though improved COP modeling allows the optimization to procure less energy overall and to operate the SOC closer to its lower limit.

Fig. 19 shows the minimal room temperature (upper diagram) for the component modeling depths $HP_{(2,3)}$-$HP_{(5,3)}$. Especially at low ambient temperatures, the deviation from the 21 °C set-point increases. With a more accurate COP representation, the optimization exploits the flexibility corridor more effectively, leading to a systematically lower SOC and thus to lower system temperatures. However, at low ambient temperatures the building requires a higher minimum storage temperature to maintain sufficient heating capacity. In the proposed framework, this effect is captured through the dynamic lower SOC bound (cf. Section 3.3), which increases the minimum admissible storage temperature as a function of outdoor conditions. If this dynamic behavior is not represented adequately, the controller may operate the BST too close to its static lower bound, resulting in insufficient thermal output and a drop below the comfort temperature. Therefore, a sufficiently high model quality is essential to map the thermodynamics with the accuracy required to fully and safely exploit the available flexibility.

The use of the disaggregation controller shows no significant deviation from the results obtained with component-level modeling. This demonstrates, first, that the optimization outcome is largely independent of the chosen aggregation level and, second, that the controller correctly reconstructs physically consistent setpoints for the individual units. In addition, the aggregated modeling approach enables the controller to mitigate component-specific load differences during runtime, leading to a more efficient utilization of the procured energy.

In summary, performance improves with increasing model accuracy. Furthermore, the approach of aggregating and disaggregating BHSs and consumers proves to be effective. Especially for larger systems, this approach allows a reduction in model complexity without sacrificing accuracy. The following section examines the aspect of model complexity in more detail.

5.3. Results on computational performance

When comparing different model formulations, a key factor is the solution time of the optimization. In the following, runtime analyses regarding the presented HP formulations are provided. The tests were carried out on an office workstation with an AMD Ryzen Threadripper PRO 7955WX CPU. In the majority of cases, Gurobi 12 is used to solve the models. For quadratically constrained programs with only continuous variables, CONOPT 4 is used.[7] The given values are averages over

[7] Though the solver does not guarantee to find a global optimum, the provided solutions have been shown to be reasonably good (see Section 5.1).

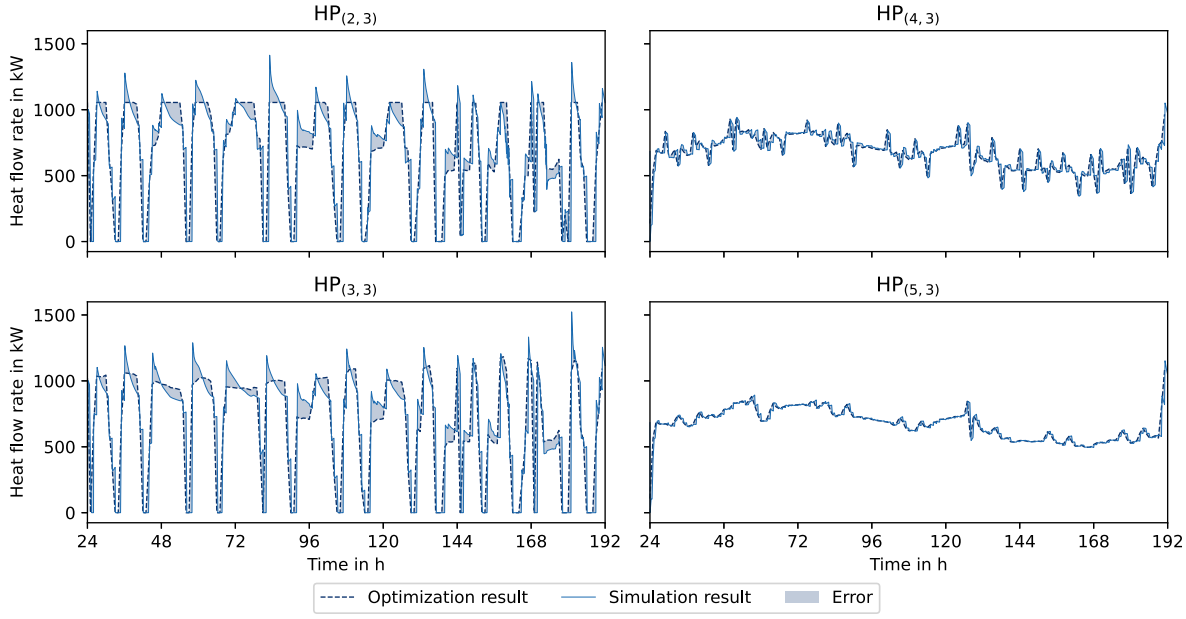

Fig. 17. Comparison of the optimized and simulated heat flow for the different component modeling depths.

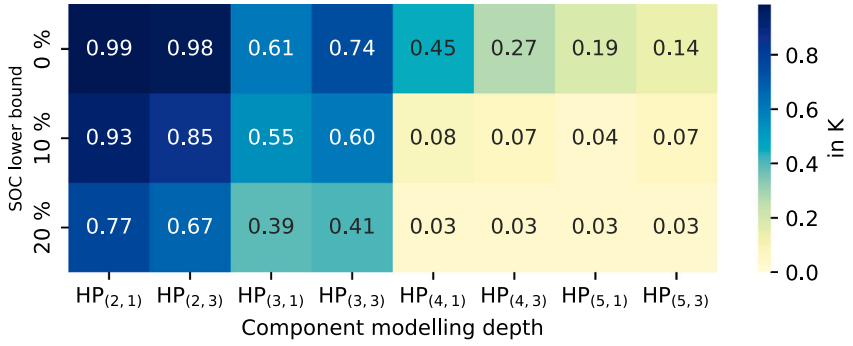

Fig. 18. Room temperature deviation from their set-point at different component modeling depths and lower SOC bounds for HP.

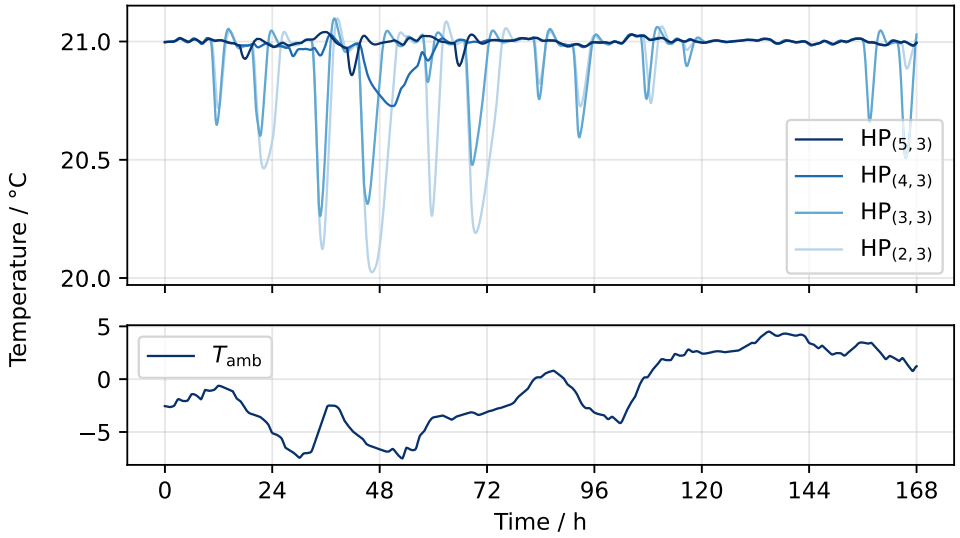

Fig. 19. Room temperature for four exemplary component modeling depths and the corresponding ambient temperature.

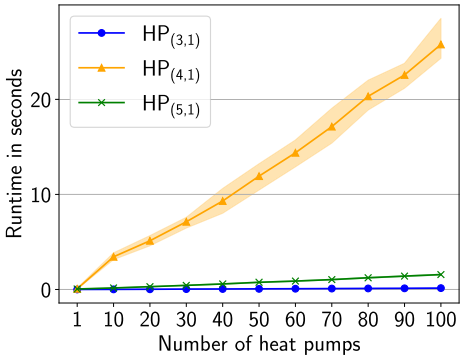

Fig. 20. Average runtimes of HP models with different numbers of BHSs considered. Within the colored area lie 90% of all measurements.

multiple test runs with sampled data from the presented case study, again spanning a time horizon of 168 time steps. First, the runtimes of the different HP representations are investigated in isolation. Later in the section, the combination with different BEV formulations is studied. Due to its similarity to $HP_{(3,\cdot)}$, $HP_{(2,\cdot)}$ is omitted.

Fig. 20 shows the runtime of the different approaches to integrate HPs in the aggregator model depending on the number of BHSs considered. For $HP_{(4,\cdot)}$, runtimes for reaching a 1% optimality gap are reported; $HP_{(3,\cdot)}$ and $HP_{(5,\cdot)}$ terminate when a (local) minimum is found. All instances were solved within the given time limit of 5 minutes. For a single HP, all formulations are solved within a fraction of a second, with Gurobi reporting close to 0 s for $HP_{(3,1)}$, while $HP_{(4,1)}$ and $HP_{(5,1)}$ take 0.05 and 0.06 s on average respectively. When increasing the problem size to the scale of the presented case study, models with an exogenous COP are solved to optimality in 0.15 s and non-linear models in 1.56 s on average. In contrast, models with an approximation of the SOC-COP relation do not scale as well with increasing problem size. The increasing complexity and variable count caused by the additional integer variables per HP unit lead to a runtime of approximately 25 s on average until a proven optimality gap of 1% is reached when considering 100 HPs.

As each component operates independently in this case study, they can be optimized in individual models. When a linked operation and therefore one holistic model is required, e.g., by introducing a total power limit over all units, runtimes are highly dependent on the specific configurations. In the following, runtimes for a model integrating HP and BEV formulations are discussed. First, the components are still not directly linked, to observe some effects of integrated models. To compare the results of adding different BEV formulations to the HP models, each BEV is mapped to the corresponding BHS according to the data of the case study. Fig. 21 shows the effect on runtimes the different combinations have considering a single household, while Table 5 summarizes

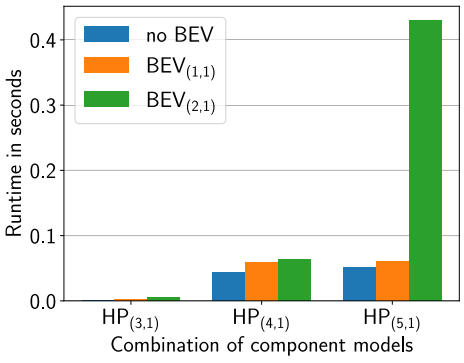

Fig. 21. Average runtimes for models combining different HP and BEV formulations for a single household.

the results for larger instances (10 and 50 households). The time limit for the following optimization runs is 1 hour. Models with $HP_{(4,\cdot)}$ terminate when an optimality gap of 1% or the time limit is reached. For MIQCPs, the optimality gap is set to 2%. Including $BEV_{(1,\cdot)}$ in a model adds only continuous variables and linear constraints. The increased problem size leads to higher runtimes in all cases, with the longest solution time being about 14 s in the case of 50 households in the $HP_{(4,\cdot)}$ configuration. When considering BEVs in the form of $BEV_{(2,\cdot)}$, problems using $HP_{(3,\cdot)}$ and $HP_{(5,\cdot)}$ are extended by integer variables, changing the program class compared to previously discussed models. An overview of the combinations and program classes can be seen in Table 6. For models using the combination $HP_{(3,\cdot)}$ and $BEV_{(2,\cdot)}$ runtimes are about doubled compared to simpler BEV representation. However, considering instances of 50 households are solved in less than a second, the absolute additional time is small. Problems considering HPs as $HP_{(4,\cdot)}$ already incorporated integer variables. The runtime from $BEV_{(1,\cdot)}$ to $BEV_{(2,\cdot)}$ increases by less than 10%. Combining the non-linear model formulations of $HP_{(5,\cdot)}$ with the mixed-integer formulation of $BEV_{(2,\cdot)}$ has the implication that CONOPT can no longer be used as a solver. Instead, Gurobi is used to solve the problem. The runtimes for these models show great variance across the instances. While the optimization for single household instances takes less than a second with moderate absolute variance, larger problem sizes with 10 households range from 1.6 s to over 450 s. No instance with 50 households reached the desired optimality gap within the time limit. On average, these runs report an optimality gap of about 5% at termination.

The previously discussed models still do not enforce a dependent operation of all components. In the following, a constraint is added that limits the total power consumption over all HPs and BEVs. The total power is not allowed to exceed 90% of the sum of the nominal powers of all HPs. The rest of the model is unchanged and time limits and optimality gaps apply as before. Refer again to Table 5 for an overview of the results. For the case of $HP_{(3,\cdot)}$, the additional constraint increases the size of the constraint matrix and leads to longer solution times. Contrary to that, runtimes for models with $HP_{(4,\cdot)}$ are reduced (at least for larger instances), as a smaller search space and stronger LP relaxations allow for a faster convergence. An exception are the single household models, in which the coupling of variables outweighs the above mentioned benefits of the new constraints. While the power limit shows a similar

Table 5
Runtimes of different model combinations. *The solution process for one of the instances terminated due to the time limit and is excluded as an outlier.

HP formulation	n	BEV formulation	runtime in seconds			
			without load limit		with load limit	
			average	median	average	median
$HP_{(3,\cdot)}$	1	$BEV_{(1,\cdot)}$	0.002	0.002	0.003	0.002
		$BEV_{(2,\cdot)}$	0.005	0.005	0.01	0.009
	10	$BEV_{(1,\cdot)}$	0.02	0.019	0.035	0.034
		$BEV_{(2,\cdot)}$	0.042	0.042	0.096	0.096
	50	$BEV_{(1,\cdot)}$	0.102	0.101	0.264	0.267
		$BEV_{(2,\cdot)}$	0.212	0.21	0.78	0.761
$HP_{(4,\cdot)}$	1	$BEV_{(1,\cdot)}$	0.059	0.05	0.093	0.06
		$BEV_{(2,\cdot)}$	0.063	0.055	5.796	0.143
	10	$BEV_{(1,\cdot)}$	3.059	3.097	0.455	0.451
		$BEV_{(2,\cdot)}$	3.081	3.115	0.932	0.915
	50	$BEV_{(1,\cdot)}$	12.612	12.806	4.415	4.405
		$BEV_{(2,\cdot)}$	13.52	13.578	6.431	6.409
$HP_{(5,\cdot)}$	1	$BEV_{(1,\cdot)}$	0.060	0.059	0.073	0.067
		$BEV_{(2,\cdot)}$	0.430	0.078	*5.543	1.825
	10	$BEV_{(1,\cdot)}$	0.373	0.374	0.733	0.713
		$BEV_{(2,\cdot)}$	101.602	1.79	29.049	0.938
	50	$BEV_{(1,\cdot)}$	4.085	4.047	10.688	10.692
		$BEV_{(2,\cdot)}$	3600	3600	1047.928	1219.219

Table 6
Overview of program classes depending on combinations of model formulations. (LP: linear program, MILP: mixed-integer linear program, QCP: quadratically constrained program, MIQCP: mixed-integer quadratically constrained program).

		BEV formulation		
		no BEV	$BEV_{(1,\cdot)}$	$BEV_{(2,\cdot)}$
HP formulation	$HP_{(3,\cdot)}$	LP	LP	MILP
	$HP_{(4,\cdot)}$	MILP	MILP	MILP
	$HP_{(4,\cdot)}$	QCP	QCP	MIQCP

effect on combination $HP_{(5,\cdot)}/BEV_{(1,\cdot)}$ compared to $HP_{(3,\cdot)}$, the beneficial effect of the new constraint on the solution process of models with integer variables can also be observed for the combination of the non-linear HP model and $BEV_{(2,\cdot)}$. In fact, while large instances could not be solved within the time limit for independent operation, limiting total power allows for all instances to reach a 2% optimality gap in about 20 minutes in the median. For some instances, a solution at the root node with the desired optimality gap can be found, which leads to runtimes below 10 s. However, the branching in the solution process is time expensive.

6. Conclusion

Energy researchers employ different forms of flexibility representation in optimization and simulation tools, depending on their specific needs and research focus. These differing approaches can significantly influence model outcomes. From the literature, two main types of model simplifications can be distinguished: (a) the level of detail used to represent individual energy technology components, and (b) the degree of aggregation applied when grouping multiple technologies into fleets. Therefore, understanding the implications of each representation form is highly important, particularly when models are used to inform policy and engineering decisions.

A general insight from this research is that errors arising from less detailed single-component representations have a greater impact on model outcomes than the degree to which individual technologies are aggregated into fleets. This finding holds for techno-economic indicators, such as dispatch costs, and engineering outcomes, such as component efficiencies and therefore energy turnover. Interestingly, aggregation of individual components into fleets can be beneficial in certain applications, as it balances out representation errors at the unit level.

In their daily work, modelers often face computational constraints that require simplifications in the representation of flexibility, even when the research question would benefit from greater model detail. Given the comparatively lower errors associated with technology aggregation, this strategy may be preferable to reducing component-level detail in practice. This is particularly true when integer-based models incorporate additional non-linear relationships for better component detail representation: aggregation can reduce the number of non-linear variables while still remaining closely aligned with physical behavior.

A particularly striking insight arises from modeling HPs, specifically regarding their coefficient of performance. Assuming a static COP, common in many market model applications, leads to overestimating the flexibility that can be utilized when wholesale price signals drive optimization outcomes. In contrast, model-endogenous formulations, where the COP is treated as a variable rather than a fixed parameter, do not exhibit this bias. Simply put, charging a thermal storage via a HP for price-arbitrage increases the storage temperature, which in turn decreases the HP's efficiency. Accounting for this techno-economic relationship results in lower flexibility potentials in models where the COP is represented in closer alignment with its underlying physical properties.

Coupling market-based dispatch models with engineering-oriented simulations of component behavior reveals an important but challenging relationship. Since market products are typically defined at relatively low temporal resolutions (e.g., hourly or quarter-hourly prices in day-ahead markets), the resulting dispatch outcomes often exhibit step-like patterns at the boundaries of time segments. Engineering models commonly operate at resolutions of seconds or even finer, and must smooth these discontinuities, yielding sometimes unexpected model behavior.

Addressing these coupling challenges between market and engineering applications remains an important direction for future research.

CRediT authorship contribution statement

Béla Wiegel: Writing – review & editing, Writing – original draft, Visualization, Validation, Software, Project administration, Methodology, Investigation, Formal analysis, Data curation, Conceptualization. **Jannis Eichenberg:** Writing – review & editing, Writing – original draft, Visualization, Validation, Resources, Methodology, Investigation, Formal analysis, Data curation, Conceptualization. **Tizian Schug:** Writing – review & editing, Writing – original draft, Visualization, Validation, Resources, Methodology, Investigation, Formal analysis, Data curation, Conceptualization. **Tim Hanke:** Writing – review & editing, Writing – original draft, Visualization, Software, Methodology, Investigation, Formal analysis, Conceptualization. **Hannes Hobbie:** Writing – review & editing, Writing – original draft, Supervision, Investigation, Conceptualization. **Johannes Brunnemann:** Writing – review & editing, Methodology, Conceptualization. **Christian Becker:** Writing – review & editing, Supervision. **Dominik Möst:** Writing – review & editing, Supervision.

Funding

This research was funded by the Federal Ministry for Economic Affairs and Energy in the project "EffiziEntEE – Effiziente Einbindung hoher Anteile Erneuerbarer Energien in technisch-wirtschaftlich integrierte Energiesysteme" under the project number 03EI1050.

For the laboratory part, this research has been performed using the ERIGrid 2.0 Research Infrastructure and is part of a project that has received funding from the European Union's Horizon 2020 Research and Innovation Programme under the Grant Agreement No. 870620. The support of the European Research Infrastructure ERIGrid 2.0 and its partner DTU is very much appreciated.

Declaration of competing interest

The authors declare that they have no known competing financial interests or personal relationships that could have appeared to influence the work reported in this paper.

Data availability

Data will be made available on request.

References

[1] ERIGrid 2.0: European Research Infrastructure supporting Smart Grid and Smart Energy Systems Research. Technology development, validation and roll out – Second Edition; 2025 Available at: https://erigrid2.eu/.
[2] German Federal Network Agency (Bundesnetzagentur). SMARD – electricity market data for Germany. 2025. Available at: https://www.smard.de/.
[3] Modelica – a unified Object-Oriented language for systems modeling, Version 3.6. Available at: https://modelica.org/.
[4] Abbasi MH, Taki M, Rajabi A, Li L, Zhang J. Coordinated operation of electric vehicle charging and wind power generation as a virtual power plant: a multi-stage risk constrained approach. Appl Energy Apr 2019;239:1294–307.
[5] Agbonaye O, Keatley P, Huang Y, Odiase FO, Hewitt N. Value of demand flexibility for managing wind energy constraint and curtailment. Renewable Energy May 2022;190:487–500.
[6] Aldik A, Al-Awami AT, Sortomme E, Muqbel AM, Shahidehpour M. A planning model for electric vehicle aggregators providing ancillary services. IEEE Access 2018;6:70685–97.
[7] Amamra S-A, Marco J. Vehicle-to-Grid aggregator to support power grid and reduce electric vehicle charging cost. IEEE Access 2019;7:178528–38.
[8] An Y, Liu Y, Guo L, Li X, Li X, Jia X, Wang T, Zhang M. A matrix game-based coordinated optimisation method of distribution networks with multiple flexible resources. IET Energy Syst Integr Sep 2024;6:283–96.

[9] Avau M, Govaerts N, Delarue E. Impact of distribution tariffs on prosumer demand response. Energy Policy Apr 2021;151:112116.
[10] Bruninx K, Pandzic H, Le Cadre H, Delarue E. On the interaction between aggregators, electricity markets and residential demand response providers. IEEE Trans Power Syst Mar 2020;35:840–53.
[11] Bürger A, Bohlayer M, Hoffmann S, Altmann-Dieses A, Braun M, Diehl M. A whole-year simulation study on nonlinear mixed-integer model predictive control for a thermal energy supply system with multi-use components. Appl Energy 2020;258.
[12] Cui Y, Cheng Y, Zhu H, Zhao Y, Zhong W. Stochastic optimization for capacity configuration of data center microgrid thermal energy management equipment considering flexible resources. Int J Electr Power Energy Syst Sep 2024;160:110132.
[13] Eichenberg J, Hobbie H, Schug T. Designing incentive mechanisms for Grid-Serving Demand-Side behavior in transmission grids: exploring market equilibria through Bi-Level programming. Working paper. 2024. https://hdl.handle.net/10419/302046.
[14] Federal Republic of Germany. Building Energy Act (gebäudeenergiegesetz, GEG); 2023. https://www.gesetze-im-internet.de/geg/. BGBl. I 2020, p. 1728, last amended by Art. 1 of the Act of 16 October 2023, BGBl. I Nr. 271.
[15] Felice A, Rakocevic L, Peeters L, Messagie M, Coosemans T, Camargo LR. Renewable energy communities: do they have a business case in Flanders? Appl Energy Sep 2022;322:119419.
[16] Ferrari ML, Gini L, Di Barba P, Mognaschi ME, Sieni E. Multi-objective optimization of a polygeneration grid including thermal energy storage system. J Energy Storage Sep 2024;97:112963.
[17] Franken L, Hackett A, Lizana J, Riepin I, Jenkinson R, Lyden A, Yu L, Friedrich D. Power system benefits of simultaneous domestic transport and heating demand flexibility in great britain's energy transition. Appl Energy Jan 2025;377:124522.
[18] Georges E, Cornélusse B, Ernst D, Lemort V, Mathieu S. Residential heat pump as flexible load for direct control service with parametrized duration and rebound effect. Appl Energy Feb 2017;187:140–53.
[19] German Institute for Standardization (DIN). DIN EN 12831:2017-09: energy performance of buildings - method for calculation of the design heat load - part 1: space heating load, module m3-3; German version EN 12831-1:2017. Berlin: DIN. English version EN 12831-1:2017; 2017.
[20] Gillner M, Westphal J, Wiegel B, Steffen T, Urbansky J, Hagemeier A, Ruppert S, Heyer A, Benthin J, Hanke T, Brunnemann J, Becker C, Speerforck A. Status of the TransiEnt library: transient simulation of complex integrated energy systems. In: Proceedings of the 16Th International Modelica-FMI conference, September 8 – 10, 2025, Lucerne University of Applied Sciences and Arts (HSLU), vol. 218. Linköping University Electronic Press; Oct 2025.
[21] Ginigeme K, Wang Z. Distributed optimal Vehicle-To-Grid approaches with consideration of battery degradation cost under Real-Time pricing. IEEE Access 2020;8:5225–35.
[22] Gümrükcü E, Klemets JRA, Suul JA, Ponci F, Monti A. Decentralized energy management concept for urban charging hubs with multiple v2g aggregators. IEEE Trans Transp Electrif Jun 2023;9:2367–81.
[23] Haikarainen C, Pettersson F, Saxén H. Optimized phasing of the development of a regional energy system. Energy Sep 2020;206:118129.
[24] Herwig H. Technische thermodynamik A-Z. Hamburg: TuTech Innovation; 2008. Literaturverz. S. [530].
[25] Hoth K, Wiegel B, Schug T, Fischer K. The energy aggregator problem – a holistic mixed-integer linear programming approach. Sustain Energy Grids Netw 2025;43:101754.
[26] Hu J, Yang G, Bindner HW, Xue Y. Application of Network-Constrained transactive control to electric vehicle charging for secure grid operation. IEEE Trans Sustain Energy Apr 2017;8:505–15.
[27] Huang S, Wu Q, Oren SS, Li R, Liu Z. Distribution locational marginal pricing through quadratic programming for congestion management in distribution networks. IEEE Trans Power Syst Jul 2015;30:2170–8.
[28] Huang S, Wu Q, Oren SS, Li R, Liu Z. Distribution locational marginal pricing through quadratic programming for congestion management in distribution networks. IEEE Trans Power Syst Jul 2015;30:2170–8.
[29] Kolawole O, Al-Anbagi I. Electric vehicles battery wear cost optimization for frequency regulation support. IEEE Access 2019;7:130388–98.
[30] Krützfeldt H, Vering C, Mehrfeld P, Müller D. MILP design optimization of heat pump systems in German residential buildings. Energy and Build Oct 2021;249:111204.
[31] Langer L, Volling T. An optimal home energy management system for modulating heat pumps and photovoltaic systems. Appl Energy Nov 2020;278:115661.
[32] Maier L, Schönegge M, Henn S, Hering D, Müller D. Assessing mixed-integer-based heat pump modeling approaches for model predictive control applications in buildings. Appl Energy Nov 2022;326:119894.
[33] Meinecke S, Sarajlić D, Drauz SR, Klettke A, Lauven L-P, Rehtanz C, Moser A, Braun M. SimBench – a benchmark dataset of electric power systems to compare innovative solutions based on power flow analysis. Energies Jun 2020;13(12):3290.
[34] Meinecke S, Sarajlić D, Drauz SR, Klettke A, Lauven L-P, Rehtanz C, Moser A, Braun M. SimBench—a benchmark dataset of electric power systems to compare innovative solutions based on power flow analysis. Energies Jun 2020;13:3290.
[35] Misconel S, Zimmermann F, Mikurda J, Möst D, Kunze R, Gnann T, Kühnbach M, Speth D, Pelka S, Yu S. Model coupling and comparison on optimal load shifting of battery electric vehicles and heat pumps focusing on generation adequacy. Energy Oct 2024;305:132266.
[36] Moghadam AT, Soheyli F, Sanei S, Akbari E, Khorramdel H, Ghadamyari M. Bi-level optimization of the integrated energy systems in the deregulated energy markets considering the prediction of uncertain parameters and price-based demand response program. Energy Sci Eng Aug 2022;10:2772–93.
[37] Monsberger C, Maggauer K, Fina B, Suna D, Fuchs C, Leitner B. Profitability of biomass-based district heating considering different technology combinations and building flexibility. Renew Sustain Energy Transit Aug 2023;4:100062.
[38] Muessel J, Ruhnau O, Madlener R. Accurate and scalable representation of electric vehicles in energy system models: a virtual storage-based aggregation approach. iScience Oct 2023;26:107816.
[39] Nobis C, Kuhnimhof T. Mobilität in deutschland – MiD ergebnisbericht. Studie von infas, DLR, IVT und infas 360 (FE-nr. 70.904/15). Technical report, Bonn, Berlin: Im Auftrag Des Bundesministers Für Verkehr Und Digitale Infrastruktur; 2018.
[40] Oluleye G, Allison J, Hawker G, Kelly N, Hawkes AD. A two-step optimization model for quantifying the flexibility potential of power-to-heat systems in dwellings. Appl Energy Oct 2018;228:215–28.
[41] Olympios AV, Sapin P, Freeman J, Olkis C, Markides CN. Operational optimisation of an air-source heat pump system with thermal energy storage for domestic applications. Energy Convers Manag Dec 2022;273:116426.
[42] Petkov I, Mavromatidis G, Knoeri C, Allan J, Hoffmann VH. MANGOret: an optimization framework for the long-term investment planning of building multi-energy system and envelope retrofits. Appl Energy May 2022;314:118901.
[43] Pfenninger S, Staffell I. Long-term patterns of european PV output using 30 years of validated hourly reanalysis and satellite data. Energy Nov 2016;114:1251–65.
[44] Pinto ES, Gronier T, Franquet E, Serra LM. Opportunities and economic assessment for a third-party delivering electricity, heat and cold to residential buildings. Energy Jun 2023;272:127019.
[45] Sarfarazi S, Mohammadi S, Khastieva D, Hesamzadeh MR, Bertsch V, Bunn D. An optimal real-time pricing strategy for aggregating distributed generation and battery storage systems in energy communities: a stochastic bilevel optimization approach. Int J Electr Power Energy Syst May 2023;147:108770.
[46] Sevdari K, Calearo L, Bakken BH, Andersen PB, Marinelli M. Experimental validation of onboard electric vehicle chargers to improve the efficiency of smart charging operation. Sustain Energy Technol Assess Dec 2023;60:103512.
[47] Shakerighadi B, Anvari-Moghaddam A, Ebrahimzadeh E, Blaabjerg F, Bak CL. A hierarchical game theoretical approach for energy management of electric vehicles and charging stations in smart grids. IEEE Access 2018;6:67223–34.
[48] Sharifi P, Banerjee A, Feizollahi MJ. Leveraging owners' flexibility in smart charge/discharge scheduling of electric vehicles to support renewable energy integration. Comput Ind Eng Nov 2020;149:106762.
[49] Sridhar A, Thakur J, Baskar AG. A data-driven approach with dynamic load control for efficient demand-side management in residential household across multiple devices. Energy Rep Jun 2024;11:5963–77.
[50] Srinivasan A, Wu R, Heer P, Sansavini G. Impact of forecast uncertainty and electricity markets on the flexibility provision and economic performance of highly-decarbonized multi-energy systems. Appl Energy May 2023;338:120825.
[51] Steffen T, Wiegel B, Baboli PT. Impacts of distribution grid congestion management on charging efficiency of private electric vehicles. In: NEIS 2024 – conference on sustainable energy supply and energy storage systems; 2024.
[52] Stute J, Pelka S, Kühnbach M, Klobasa M. Assessing the conditions for economic viability of dynamic electricity retail tariffs for households. Adv Appl Energy Jul 2024;14:100174.
[53] Tan J, Wu Q, Zhang M. Strategic investment for district heating systems participating in energy and reserve markets using heat flexibility. Int J Electr Power Energy Syst May 2022;137:107819.
[54] Terlouw T, AlSkaif T, Bauer C, Mazzotti M, McKenna R. Designing residential energy systems considering prospective costs and life cycle GHG emissions. Appl Energy Feb 2023;331:120362.
[55] Vivian J, Croci L, Zarrella A. Experimental tests on the performance of an economic model predictive control system in a lightweight building. Appl Therm Eng Aug 2022;213:118693.
[56] Wiegel B, Steffen T, Babazadeh D, Becker C. Towards a more comprehensive open-source model for interdisciplinary smart integrated energy systems. In: 2023 11th workshop on modelling and Simulation of Cyber-Physical energy systems (MSCPES). IEEE; May 2023. p. 1–7.